Multi-Energy Soft X-ray Measurements of Tokamak Fusion Plasmas

K Tritz, D J Clayton, D Stutman,
Johns Hopkins University
R E Bell, A Diallo, B P LeBlanc, M Podesta,
Princeton Plasma Physics Laboratory
S Sabbagh, *Columbia University*, and the NSTX TEAM

APS 2013 - Denver, CO
Nov. 11th-15th

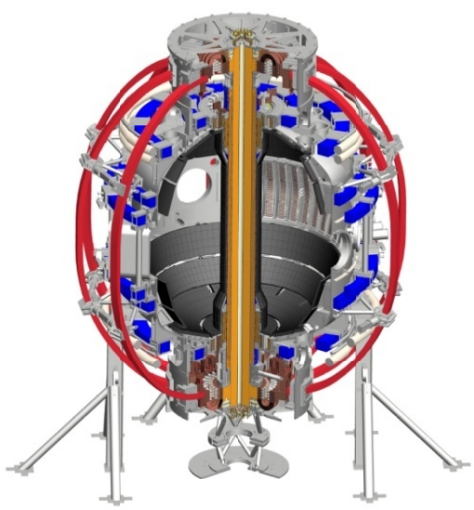

College W&M
Colorado Sch Mines
Columbia U
CompX
General Atomics
INL
Johns Hopkins U
LANL
LLNL
Lodestar
MIT
Nova Photonics
New York U
Old Dominion U
ORNL
PPPL
PSI
Princeton U
Purdue U
SNL
Think Tank, Inc.
UC Davis
UC Irvine
UCLA
UCSD
U Colorado
U Illinois
U Maryland
U Rochester
U Washington
U Wisconsin

Culham Sci Ctr
U St. Andrews
York U
Chubu U
Fukui U
Hiroshima U
Hyogo U
Kyoto U
Kyushu U
Kyushu Tokai U
NIFS
Niigata U
U Tokyo
JAEA
Hebrew U
Ioffe Inst
RRC Kurchatov Inst
TRINITI
KBSI
KAIST
POSTECH
ASIPP
ENEA, Frascati
CEA, Cadarache
IPP, Jülich
IPP, Garching
ASCR, Czech Rep
U Quebec

The Johns Hopkins spectroscopy group has developed novel SXR/XUV diagnostics for fusion plasmas

- Multi-energy Soft X-ray (ME-SXR) provides good time/spatial resolution, coarse spectral resolution

  - **High speed T_e profile measurements (~10kHz)**

  - MHD, disruption physics, ELM profile dynamics, boundary, ...

  - Impurity transport, e^- thermal transport (LBO)

- XUV/VUV Transmission grating imaging spectrometer/radiometer (TGIS/TGIR) provides good spectral/spatial resolution, coarse time resolution

  - High speed T_e profile measurement improvement

  - Divertor impurity radiation, transport & T_e (code validation)

  - Impurity transport, accumulation (e.g. non-inductive startup)

ME-SXR arrays use high time resolution diode arrays with different filters for coarse spectral resolution

- NSTX ME-SXR edge array used 4 filtered diode arrays, 1 bolometer diode array (0.3 μm Ti, 5 / 15 / 50 μm Be)
  - each diode array views same overlapping plasma volume
- 20 spatial channels provide 1 cm spatial resolution of the plasma edge (R = ~130-150cm) with >10 kHz time resolution
- Digitally controlled variable gain amplifiers optimizes ME-SXR sensitivity over wide range of plasma regimes/parameters

K. Tritz, et al.. Rev. Sci. Instrum. 83, 10E109 (2012)

Edge ME-SXR tangential mid-plane view on NSTX 2011

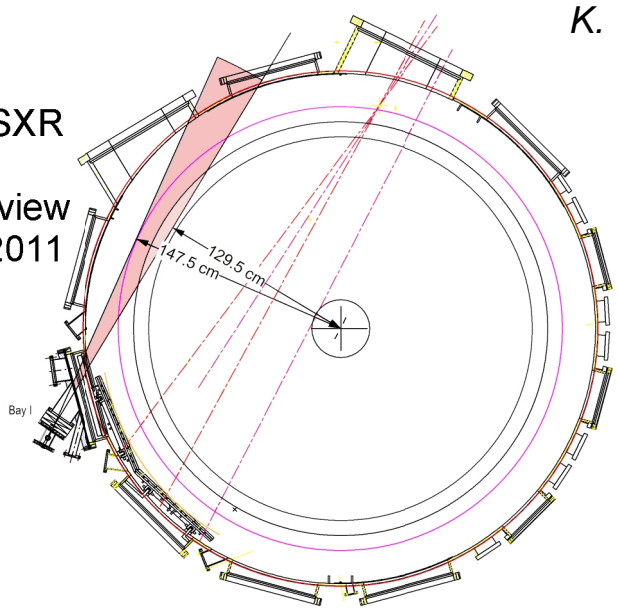

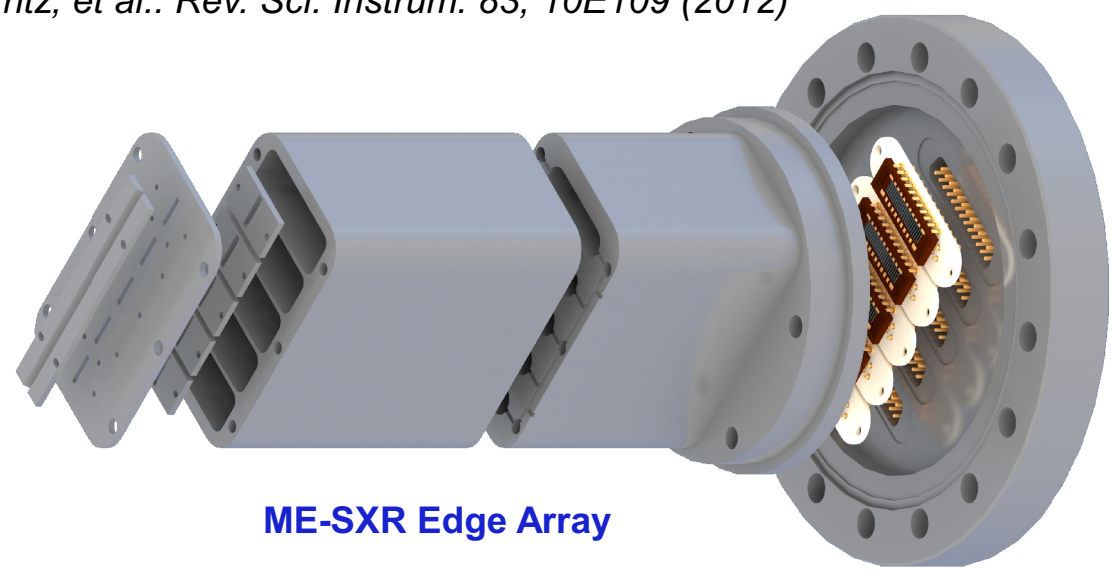

ME-SXR Edge Array

Previous work used linearization of SXR emissivity to separate contributions from n_e, n_z, T_e

- Filtered SXR emissivity E_f is function of density and concentration-weighted filtered impurity response $R_f(T_e)$

$$E_f(n_e, T_e, c) = n_e^2 \sum_i c_i R_{f,i}$$

- 2nd order linear expansion separates T_e, n_e terms (mostly)

$$\Delta E_f = \frac{\partial E_f}{\partial n_e}\Delta n_e + \frac{\partial^2 E_f}{\partial n_e^2}\frac{\Delta n_e^2}{2} + \frac{\partial E_f}{\partial T_e}\Delta T_e + \frac{\partial^2 E_f}{\partial T_e^2}\frac{T_e^2}{2} + \frac{\partial^2 E_f}{\partial n_e \partial T_e}\Delta n_e \Delta T_e$$

$$\frac{\Delta E_{f1}}{E_{f1}} - \frac{\Delta E_{f2}}{E_{f2}} = \left(\frac{\sum_i c_i R'_{f1,i}}{\sum_i c_i R_{f1,i}} - \frac{\sum_i c_i R'_{f2,i}}{\sum_i c_i R_{f2,i}}\right)\left(1 + \frac{2\Delta n_e}{n_e}\right)\Delta T_e + \left(\frac{\sum_i c_i R''_{f1,i}}{\sum_i c_i R_{f1,i}} - \frac{\sum_i c_i R''_{f2,i}}{\sum_i c_i R_{f2,i}}\right)\frac{\Delta T_e^2}{2}$$

- ME-SXR normalized difference removes most n_e dependence
  - T_e accuracy depends on calculated R, R', R'' (ADAS, CHIANTI)

Neural Networks can calculate $T_e(R,t)$ without relying on accurate atomic physics modeling

T_e from previous analytic ΔE_f

- MPTS profiles $T_e(R)$ with a 60Hz repetition rate
- Accurate atomic physics modeling of $R_{z,f}$ (CHIANTI, ADAS) allows high time resolution >10kHz $T_e(R)$ between Thomson measurements
- Large transport, non-coronal charge state distributions, atomic modeling of high-Z impurity emissivity challenges analysis

T_e from Neural Networks

- Neural networks trained with MPTS data and raw ME-SXR data
  - no atomic modeling required (or even calibrations!)
- Neural networks studied with synthetic SXR data, and successfully used with experimental ME-SXR data
- Improved results with additional diagnostics, real time $T_e(R)$ possible

A fully-connected three-layer Neural Network uses SXR and spectroscopy inputs, outputs $T_e(R)$

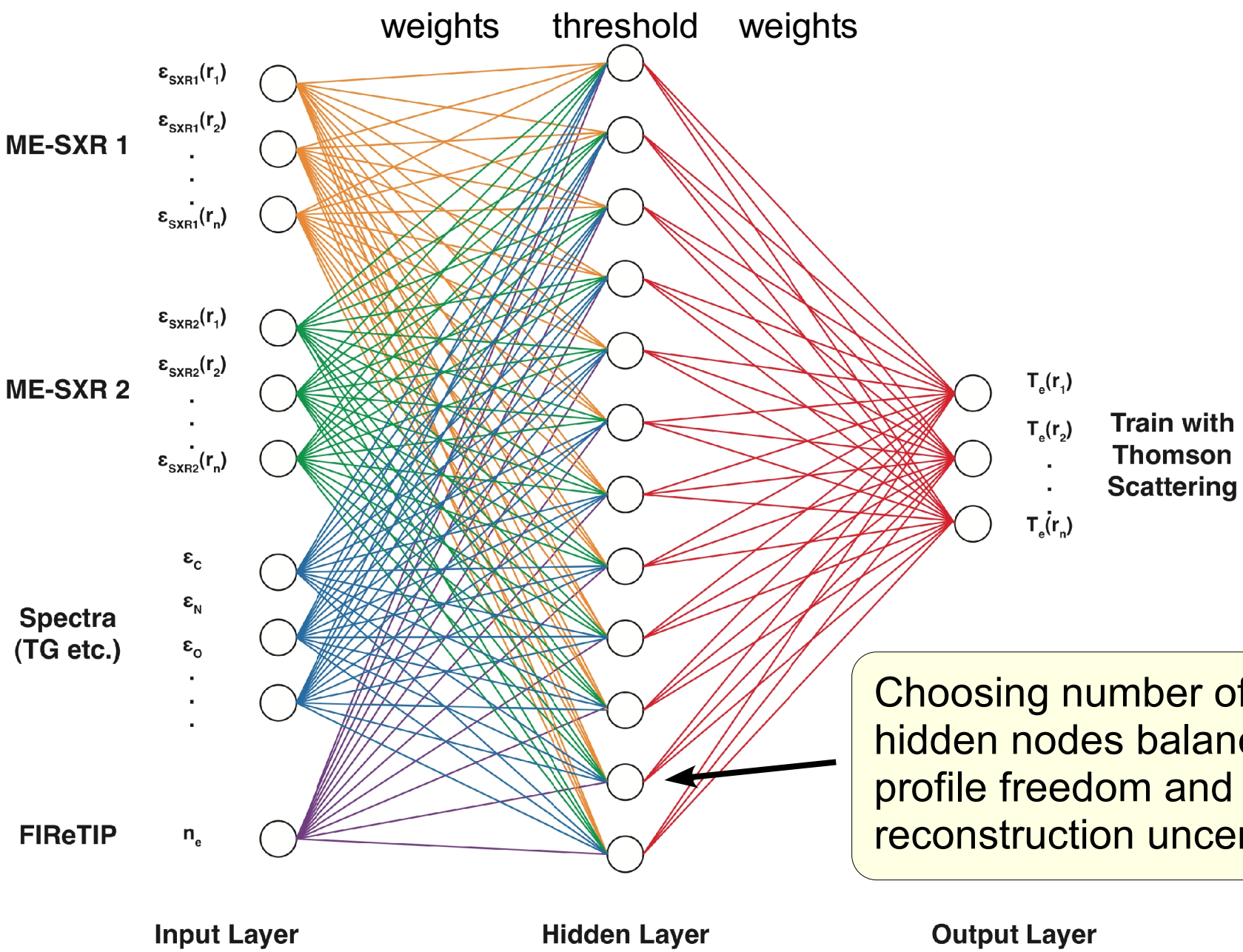

Choosing number of hidden nodes balances profile freedom and reconstruction uncertainty

Feedforward Neural Network initially tested with synthetic data to test $T_e(R)$ sensitivity and accuracy

D J Clayton et al 2013 Plasma Phys. Control. Fusion 55 095015

- PyBrain, a Python modular machine learning library used for NN
- 3-layer feedforward network used

  - number of hidden layer nodes optimized using 5x cross-validation
    40 hidden nodes generally a good choice for this study

- Rprop-learning algorithm [Igel and Hüsken, Neurocomputing 50 (2003)] used for supervised training of NN using MPTS data

  - All inputs/outputs scaled to range from 0 to 1 for improved performance using NN sigmoid threshold function

- Synthetic data for testing used real plasma profiles and SXR emissivity modeled using CHIANTI and ADAS spectrum codes

  - atomic modeling only for synthetic testing, not needed for NN $T_e(R)$

Neural Network cross-validation testing illustrates relationship between hidden nodes and T_e reconstruction error

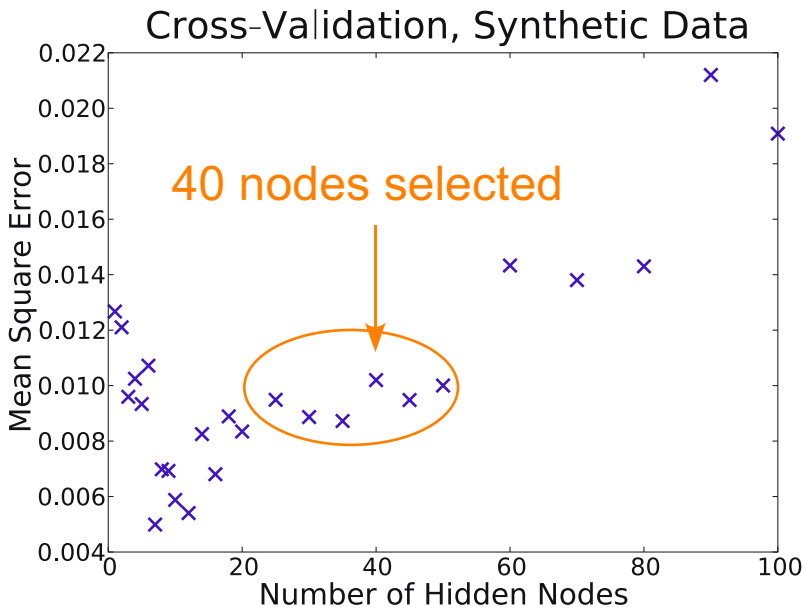

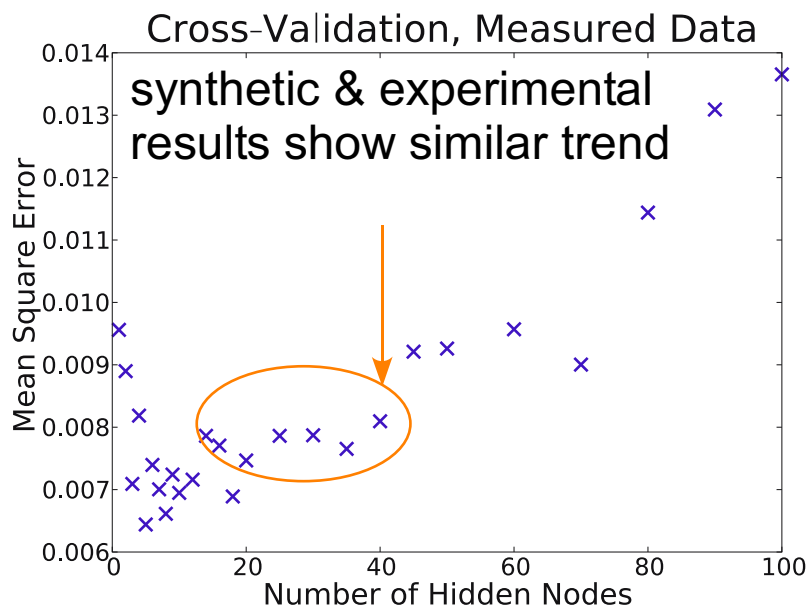

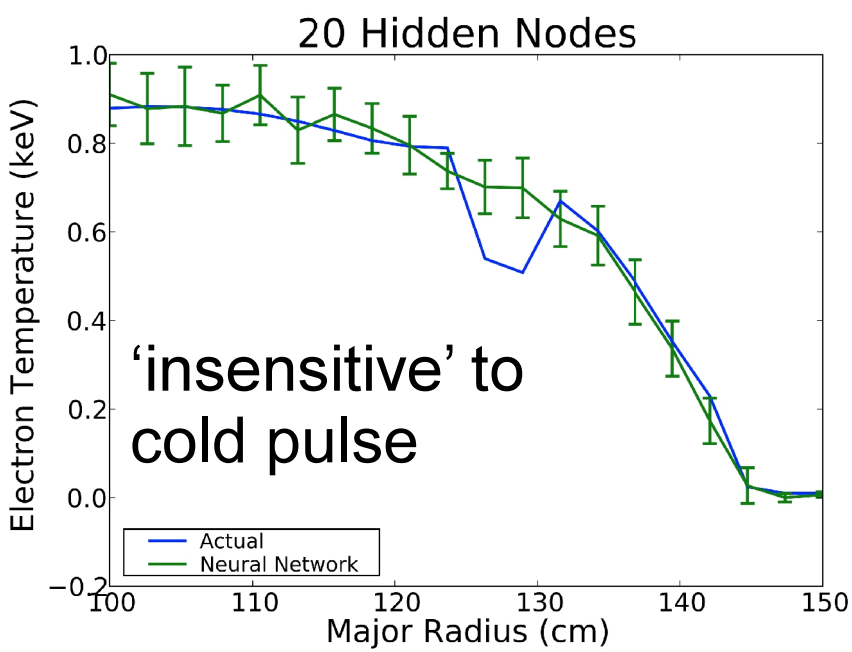

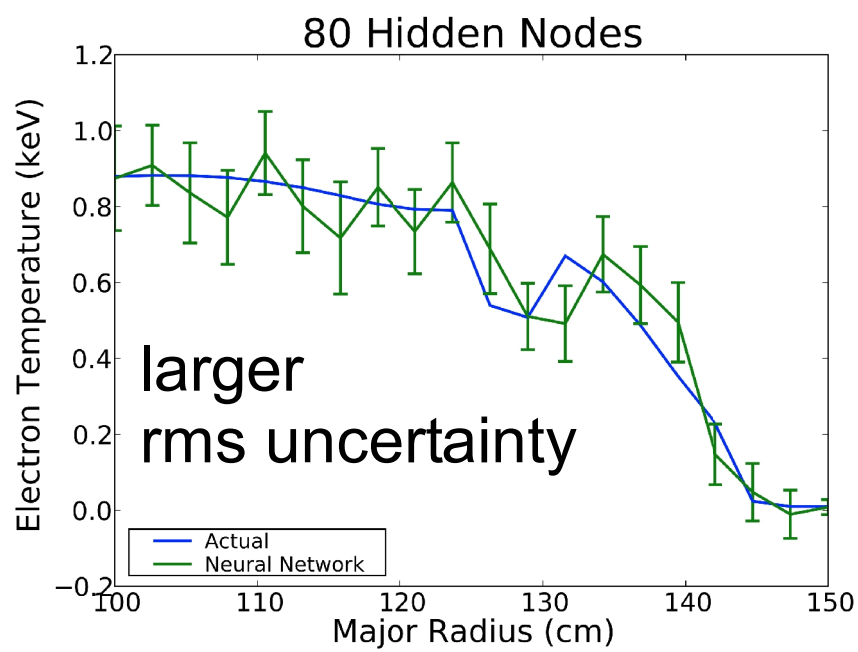

Multiple ME-SXR arrays necessary to discriminate changes in $T_e(R)$ from n_e and impurity changes

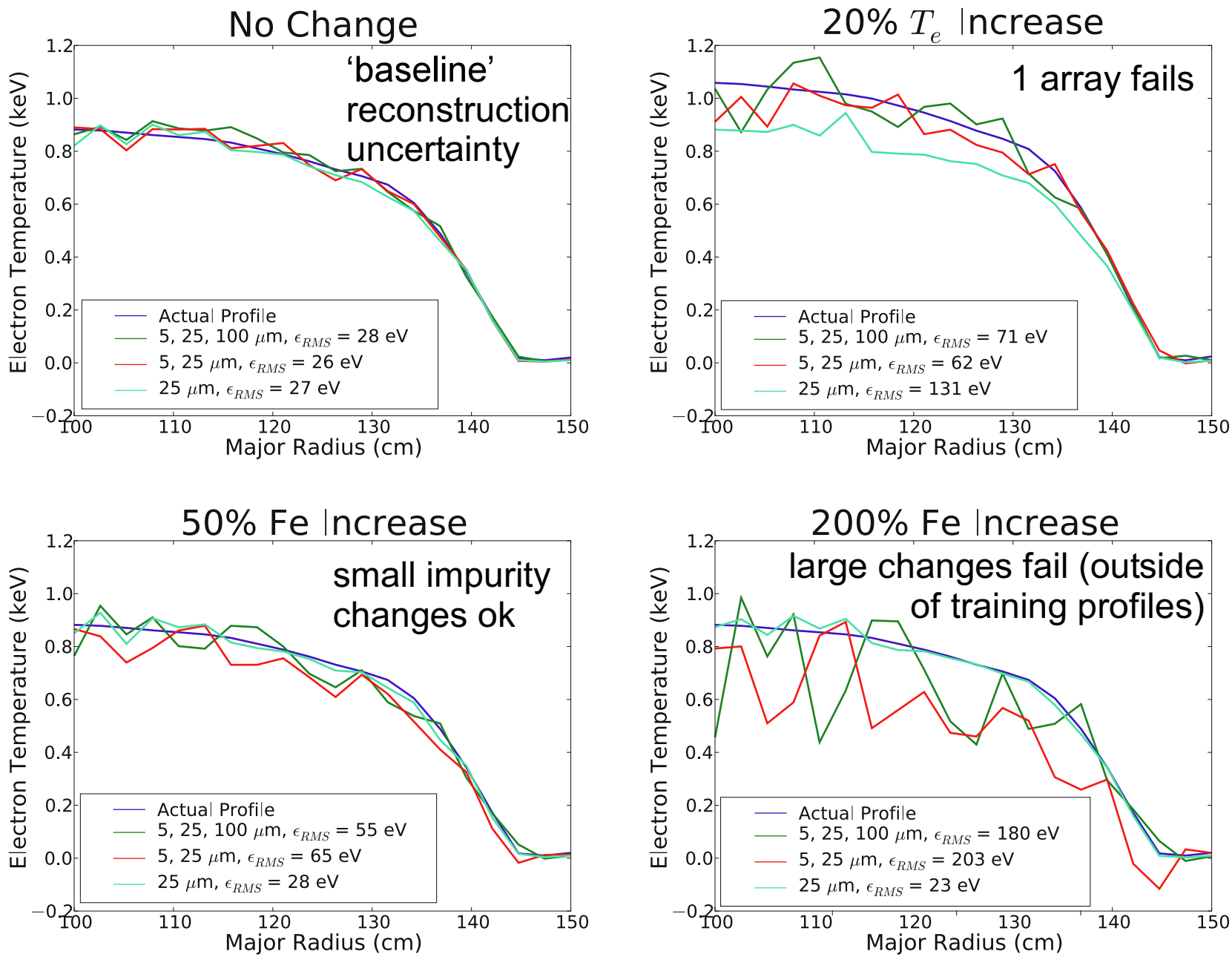

TGIS, FIReTIP diagnostics can significantly improve $T_e(R)$ Neural Network reconstruction

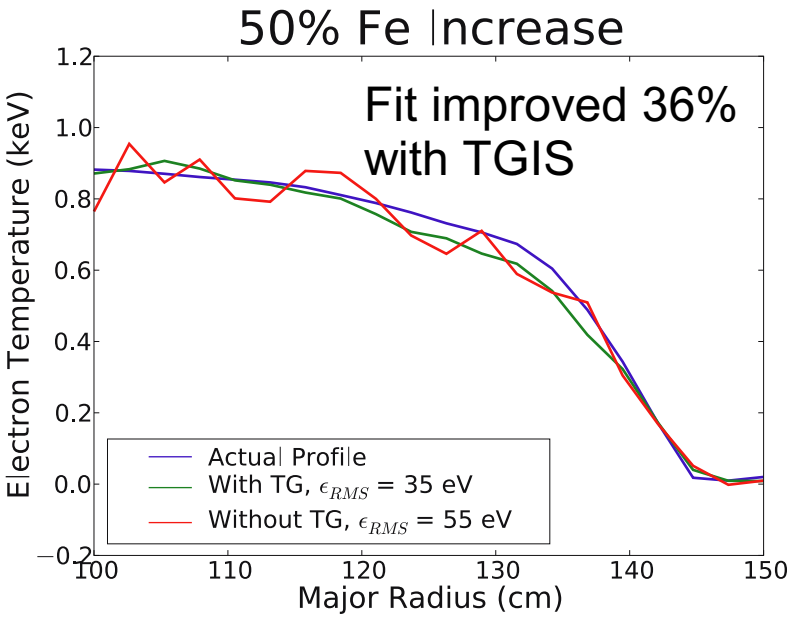

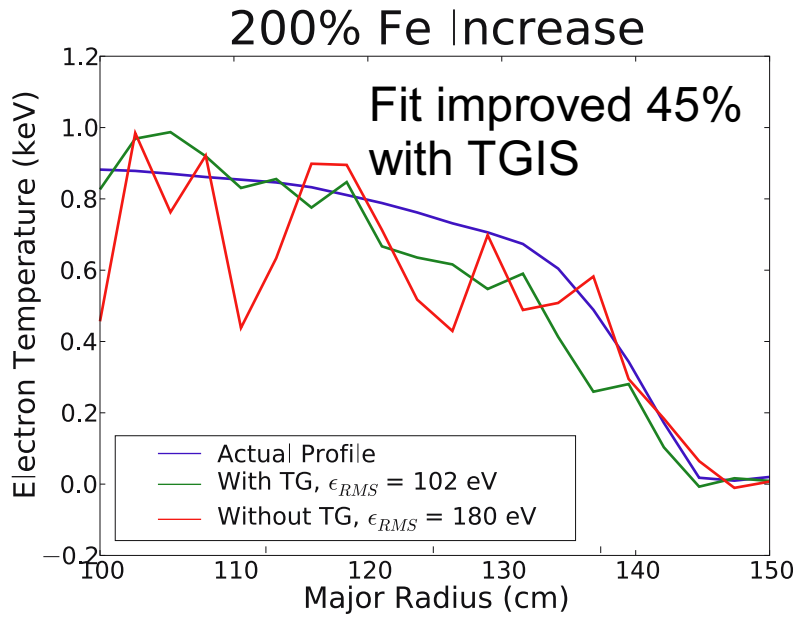

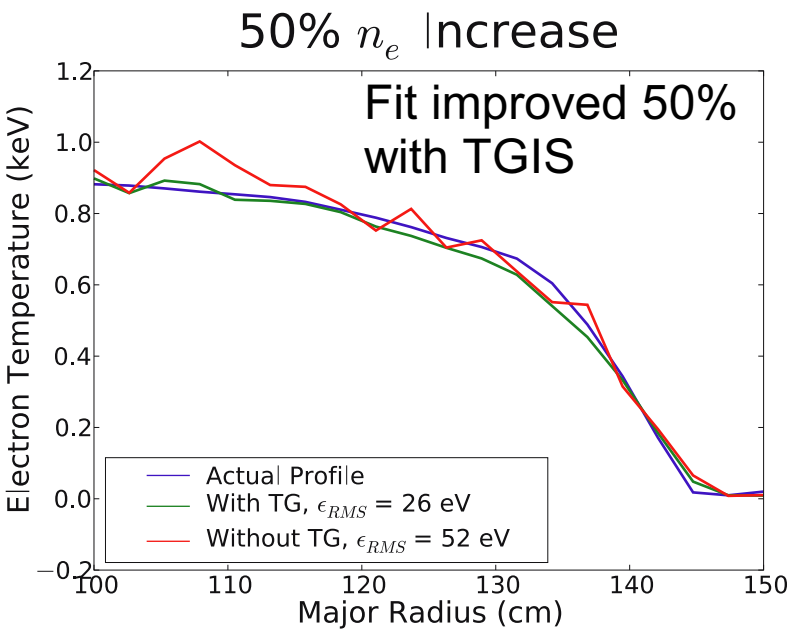

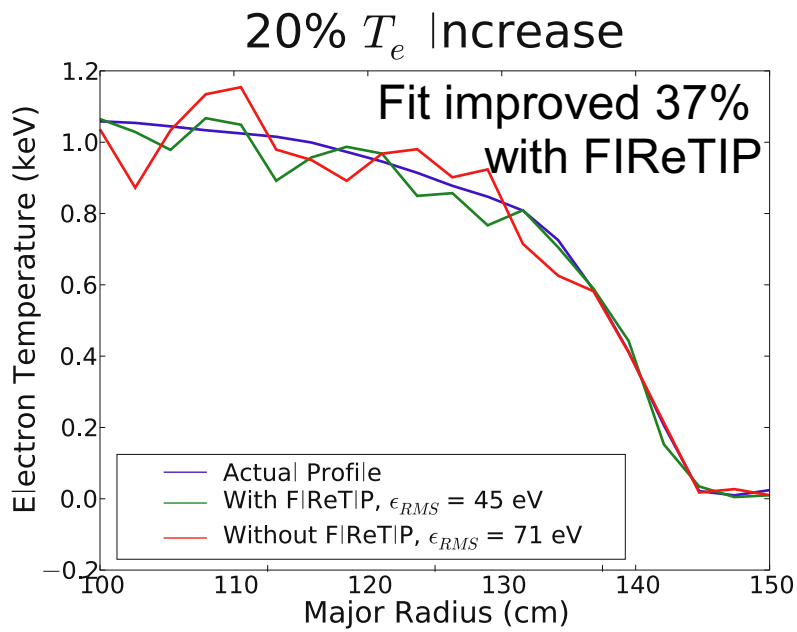

NN $T_e(R,t)$ successfully reconstructed with raw, uncalibrated data from previous generation, 3 array, optical ME-SXR*

*L F Delgado-Aparicio et al 2007 Plasma Phys. Control. Fusion 49 1245

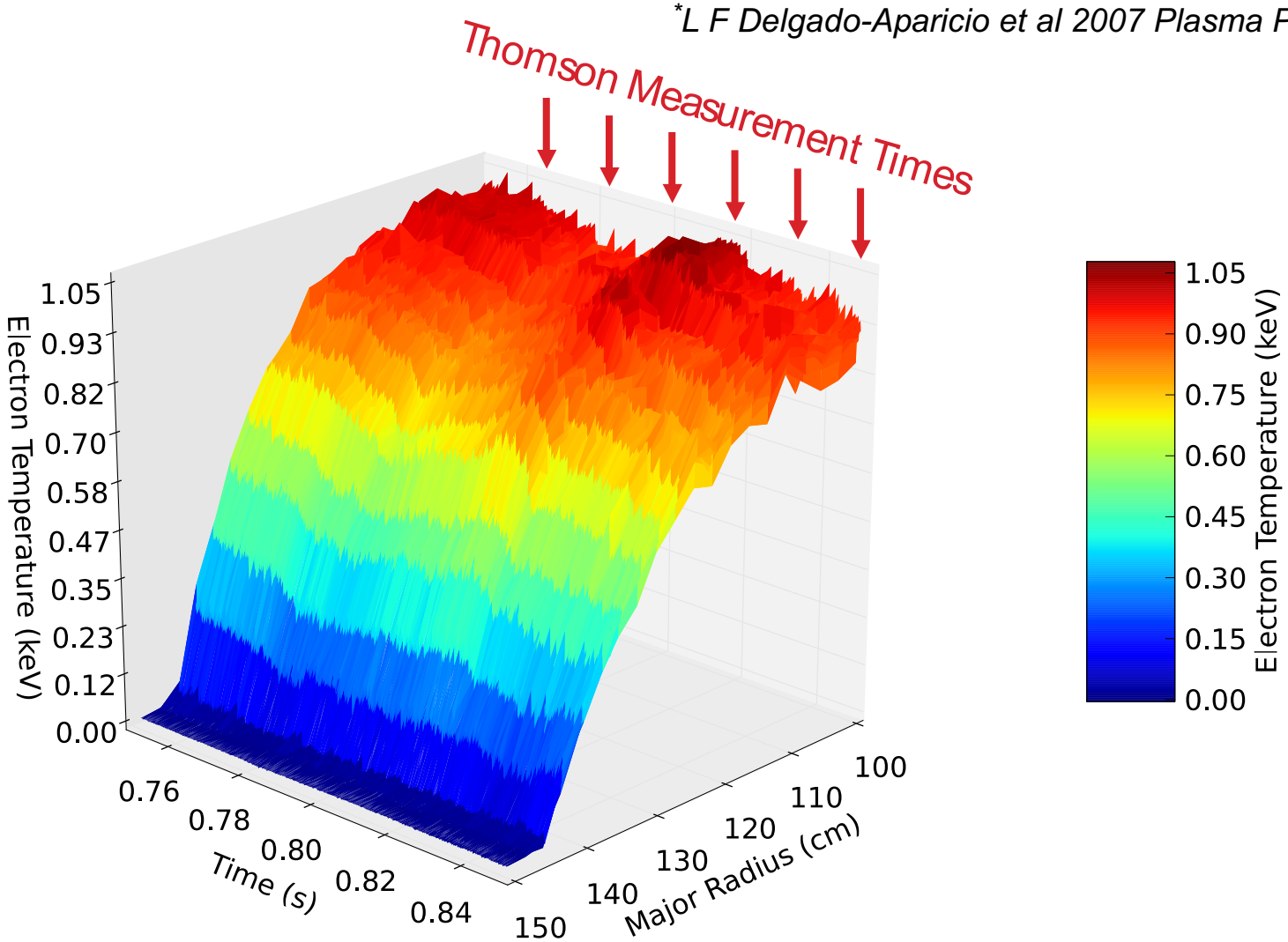

- NN trained on 30 discharges (half with Ne puffs) >1800 MPTS times - 48 input (3 arrays x 16 channels), 40 hidden, 16 output nodes

Fast NN $T_e(R,t)$ reconstruction highlights ability to measure changes missed by 60Hz MPTS system

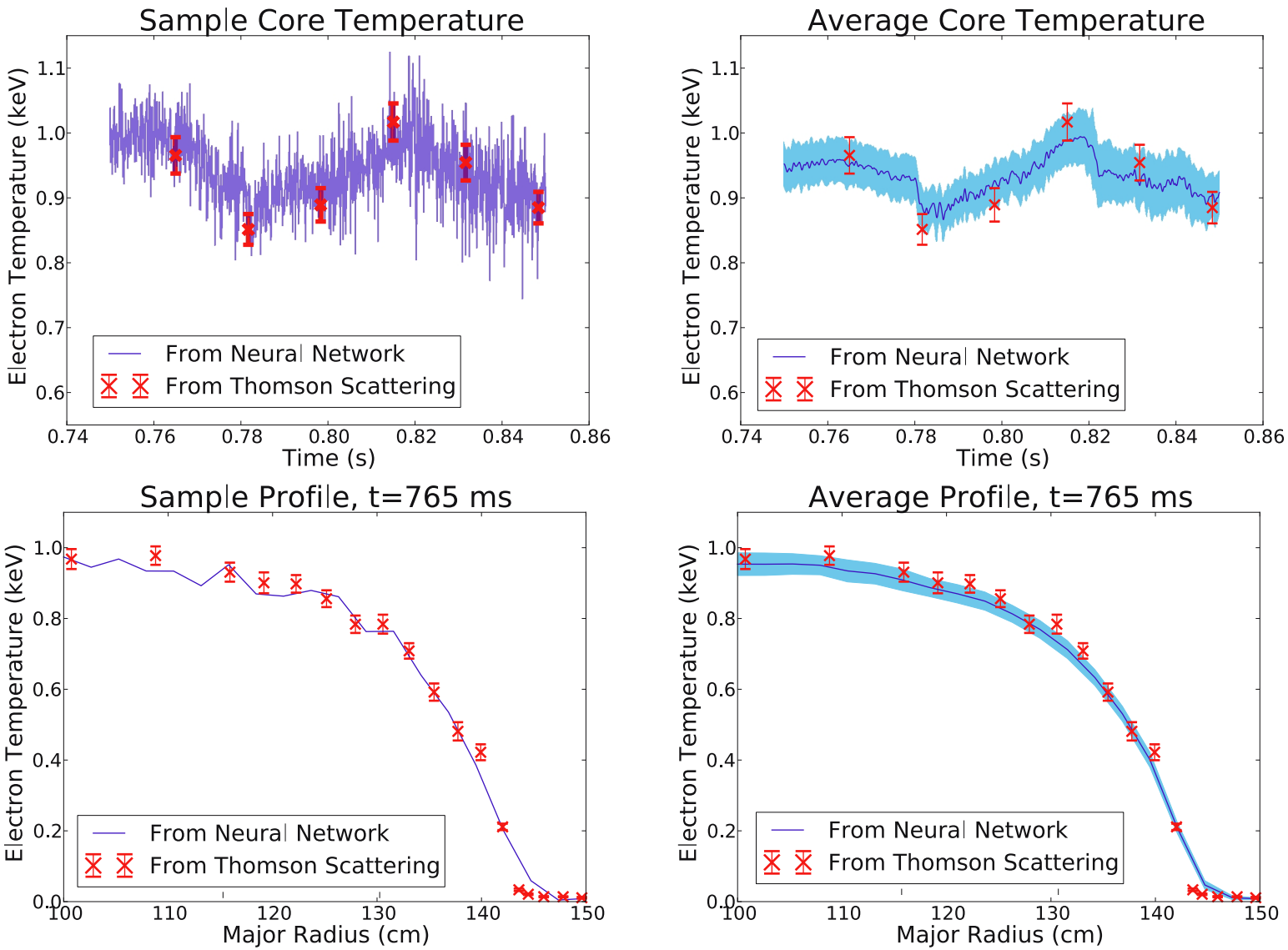

- Average profiles w/ stddev derived using ensemble fits from retraining and initializing NN 100 times with different starting connection weights

High resolution tangential ME-SXR provides improved edge measurements compared to poloidal USXR system

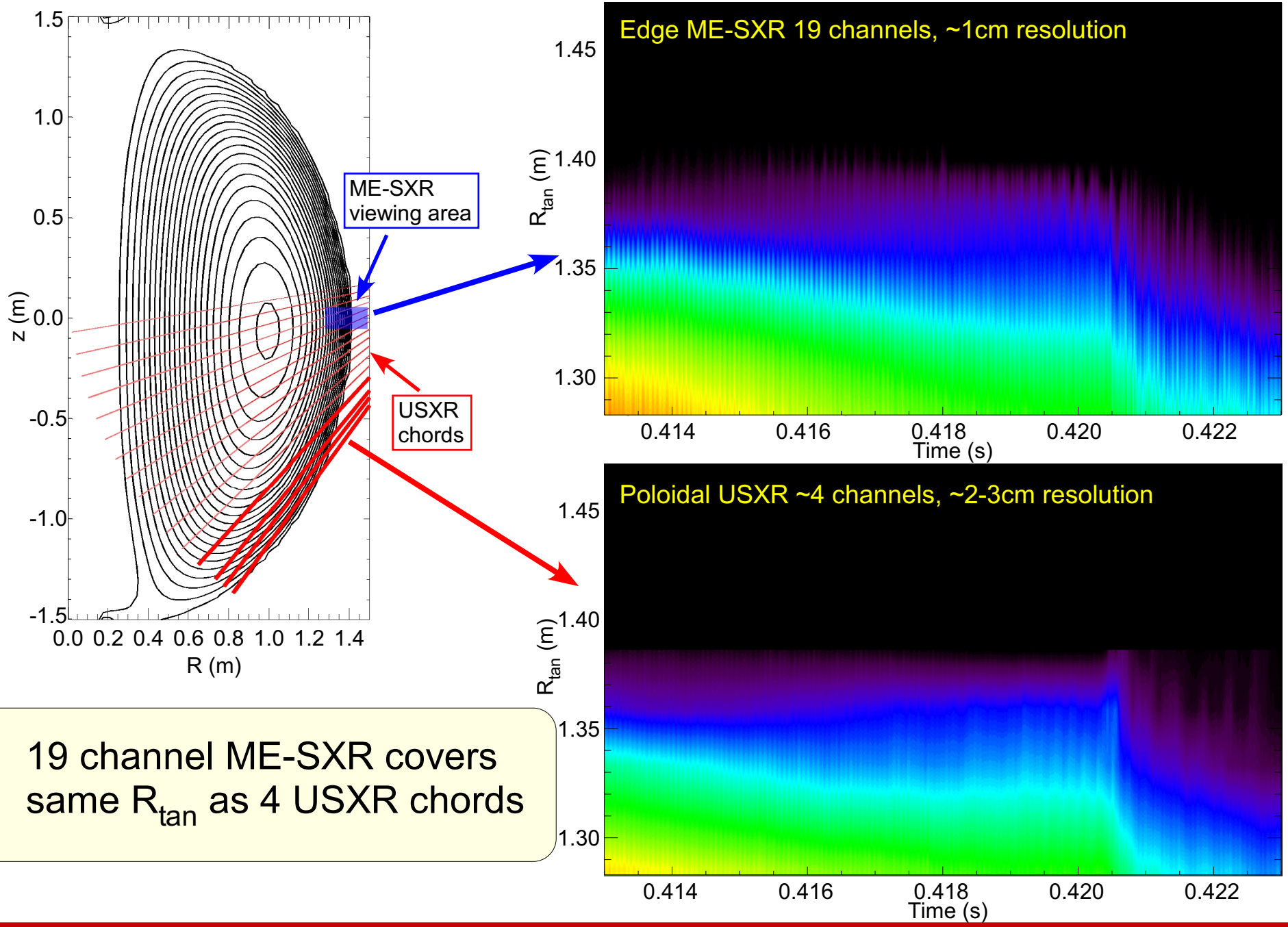

- 19 channel ME-SXR covers same R_{tan} as 4 USXR chords

Abel inversion of tangential ME-SXR data shows detailed edge dynamics before profile crash

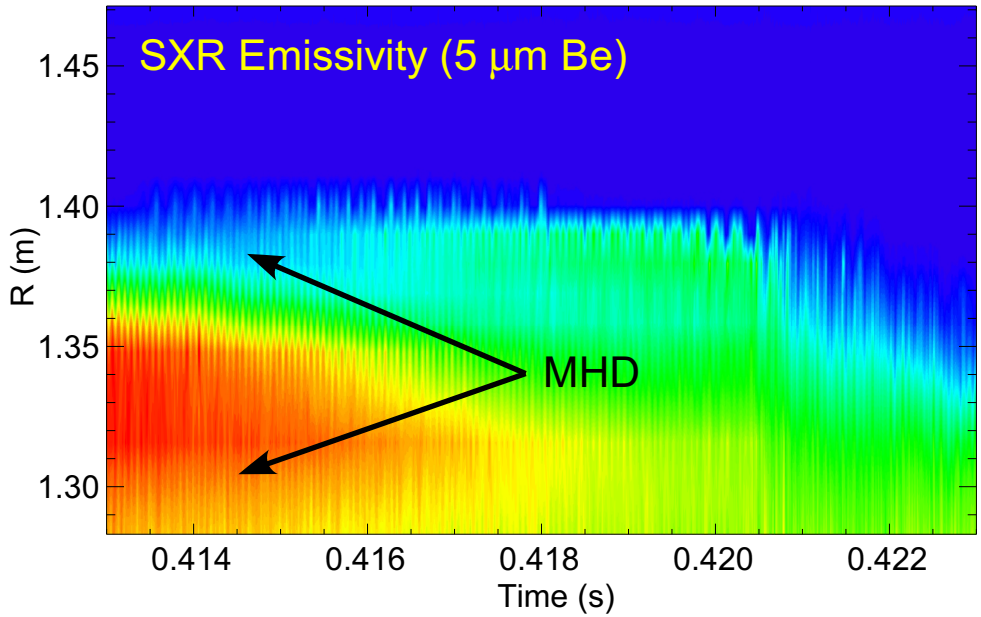

- 16 kHz internal MHD mode coupled to edge
- edge MHD slows prior to profile crash

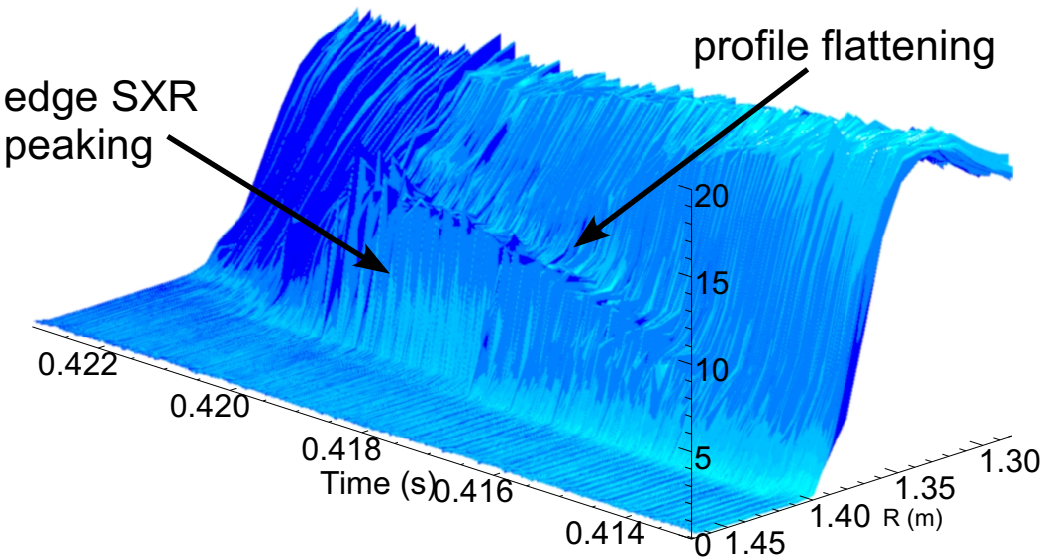

- SXR profile begins to flatten
- strong steepening of edge emission profile prior to crash (possible C accumulation, related to density limit?)

High spatial resolution measures strong localization of emission during edge MHD activity

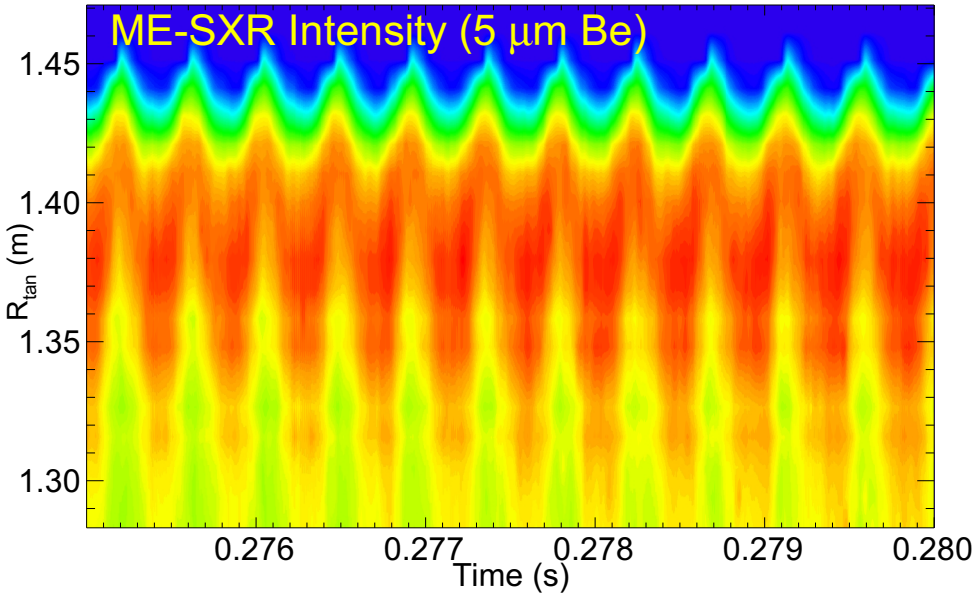

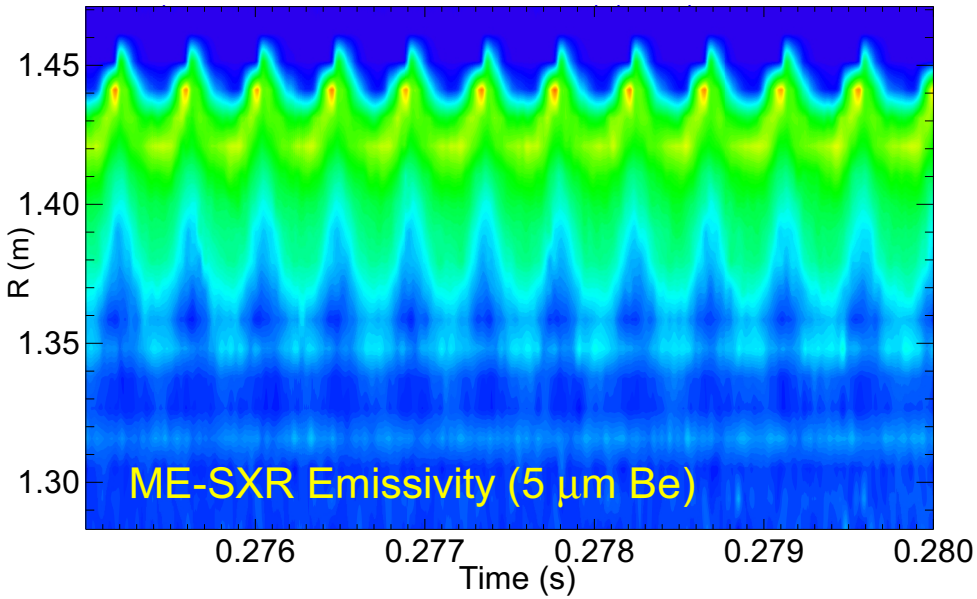

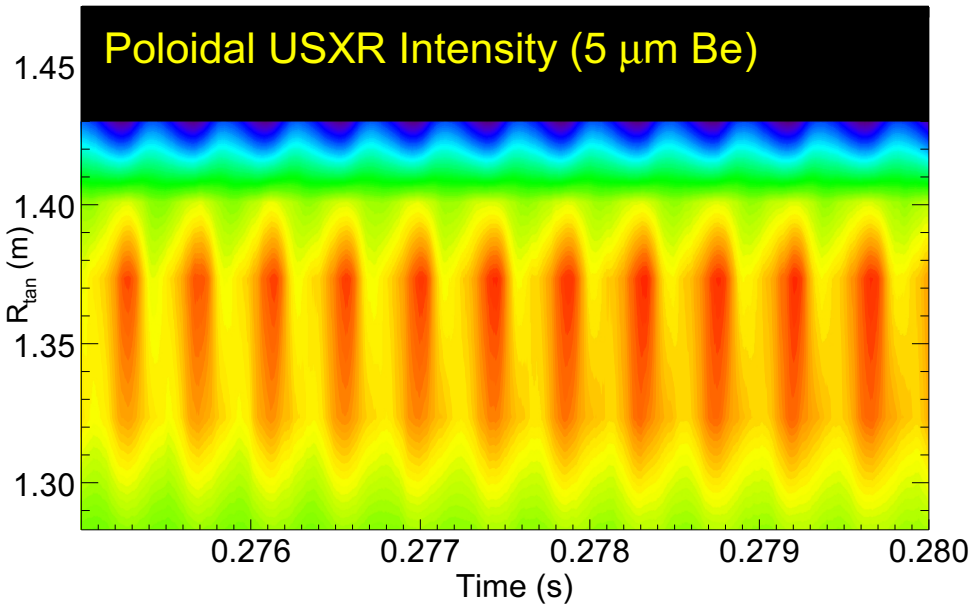

- Inversion shows highly localized MHD, Δr~1cm SXR emission near edge (possible carbon accumulation?)
- High spatial resolution and Abel inversion provide advantages over poloidal USXR system

Time/spatial resolution of ME-SXR allows investigation of different ELM cycle dynamics

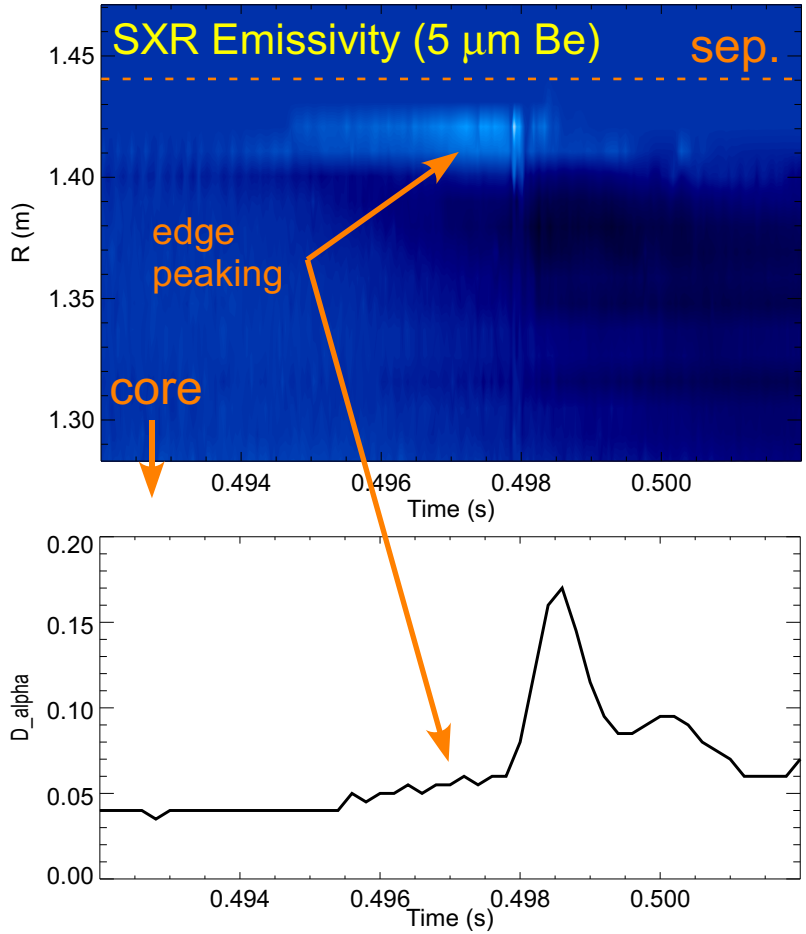

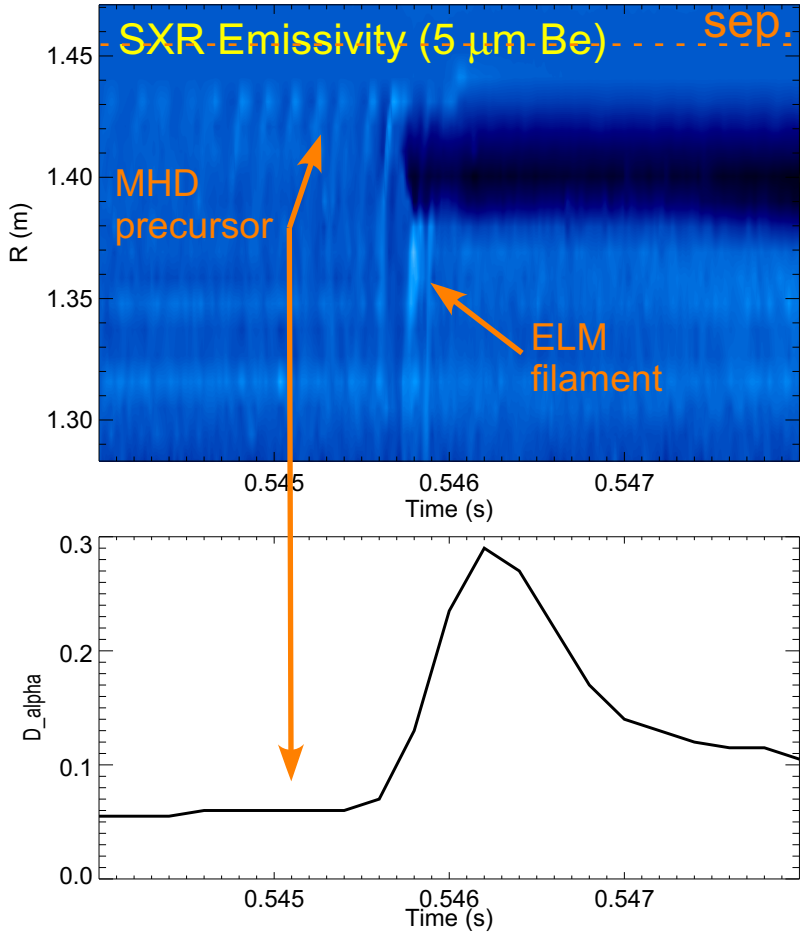

- MHD precursor leads to profile flattening, edge peaking of SXR
- ELM causes broad profile crash

- MHD precursor leads to large ELM filament
- ELM crash limited to edge

Interpolation/extrapolation of ME-SXR profiles can identify 'SXR boundary' location

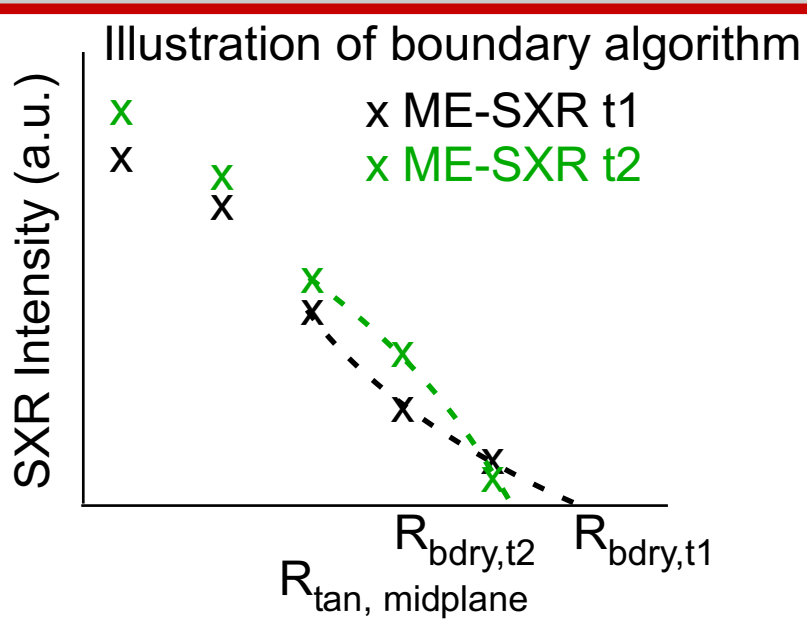

- For each time point:
  Fit quadratic/cubic polynomial to edge channels with SXR signal
- Calculate SXR boundary location from zero-crossing of polynomial

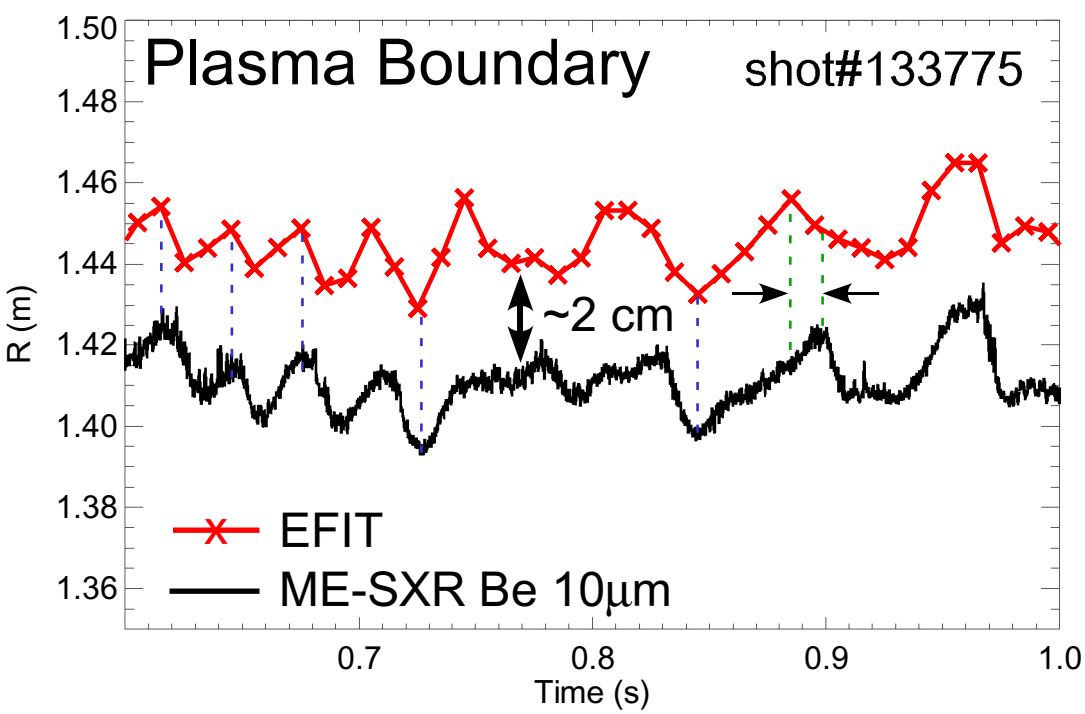

SXR boundary agrees with EFIT (+ offset from filter)

potential for ME-SXR real time pedestal gradient

Most features 'in-phase', some show phase shift
(need multiple toroidal ME-SXR)

Fast measurements of boundary location can show boundary effects of MHD (islands, kinks, RWM, ...)

2/1 tearing mode coupled to saturated core 1/1 kink

n=1 external kink/RWM

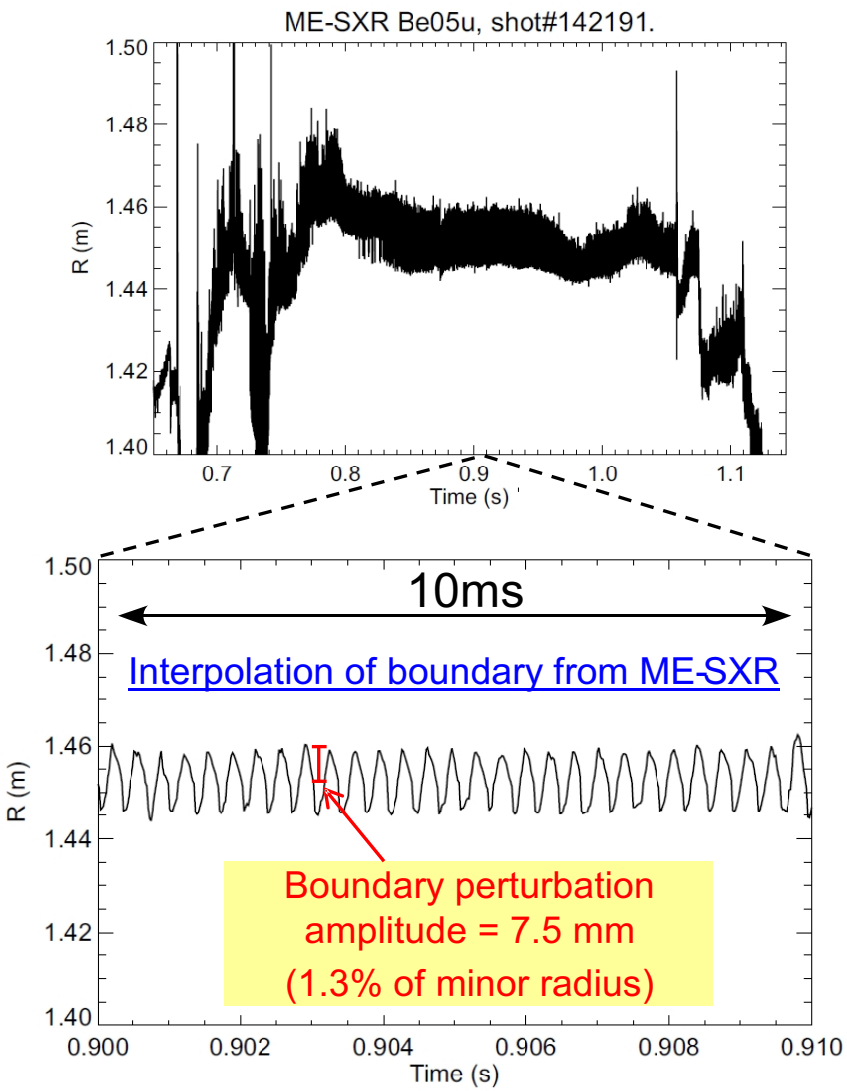

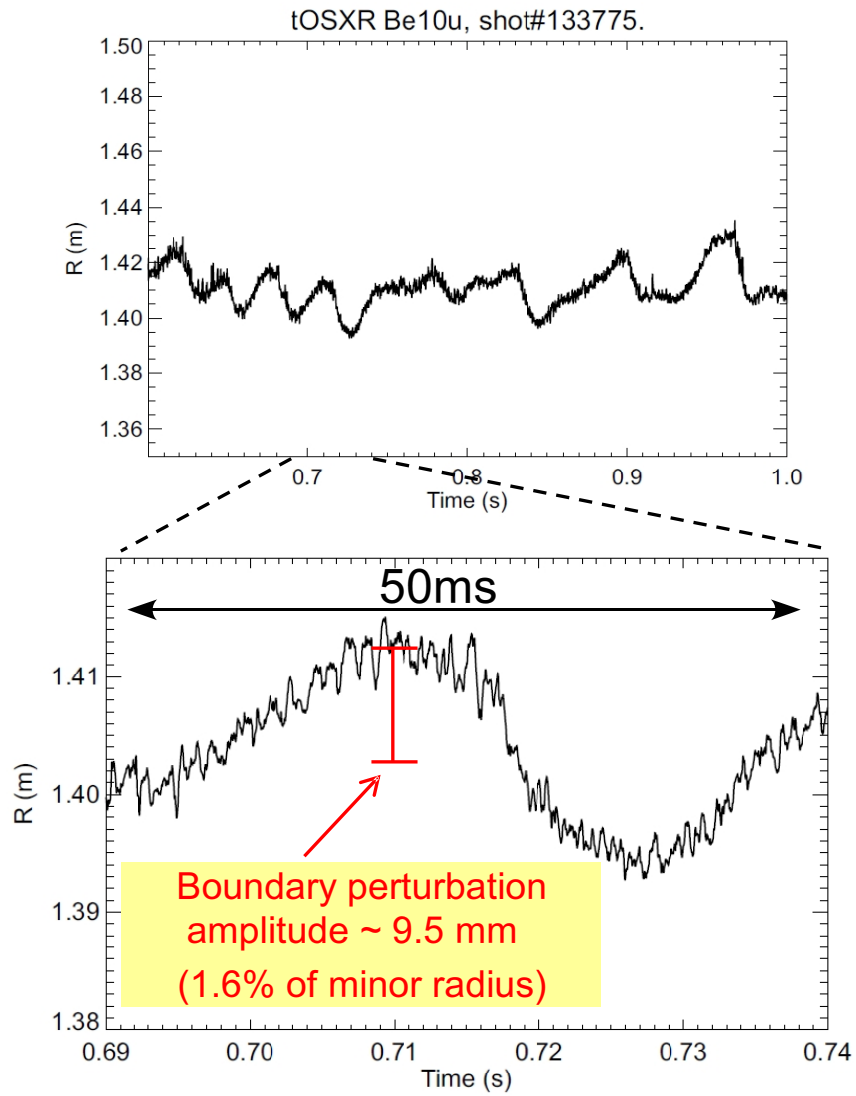

ME-SXR with active impurity seeding provides impurity transport measurements

- Neon gas puff + STRAHL transport code constrained by ME-SXR

ME-SXR filters discriminate Ne charge states

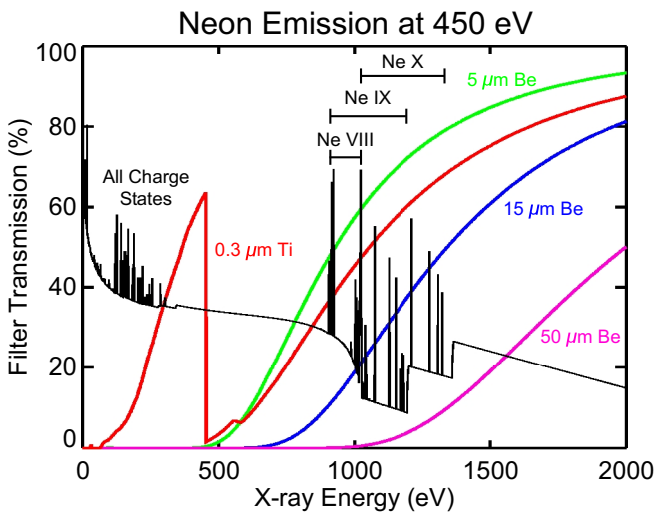

STRAHL calculated Ne radial distribution

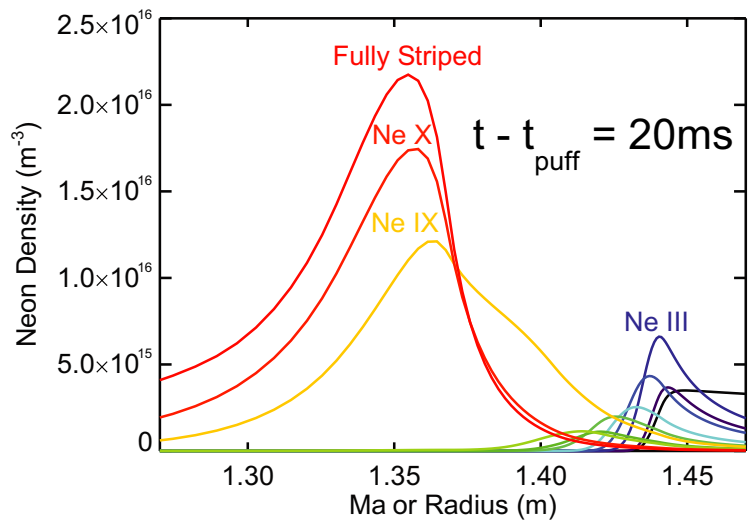

compare

ME-SXR 5μm Be neon intensity

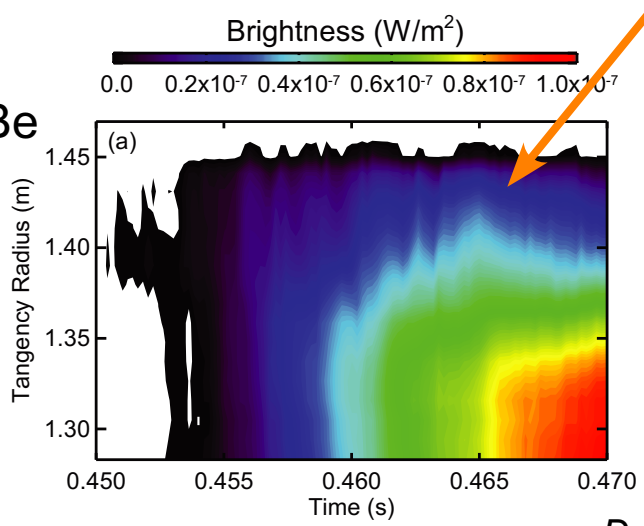

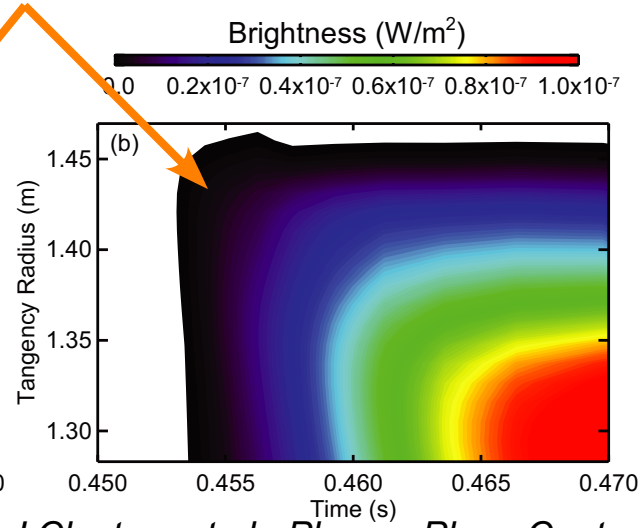

STRAHL computed neon intensity (uses ADAS)

D J Clayton, et al., Plasma Phys. Control. Fusion, 54, 105022 (2012)

Transport coefficients calculated from STRAHL time-dependent fitting of ME-SXR profiles

fit vs. time and vs. filter

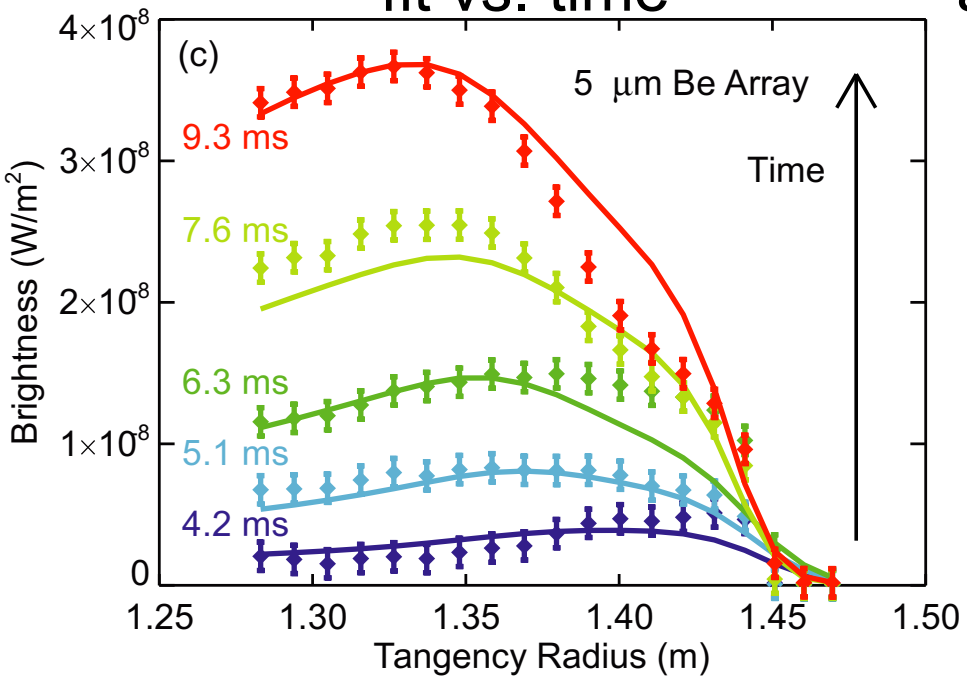

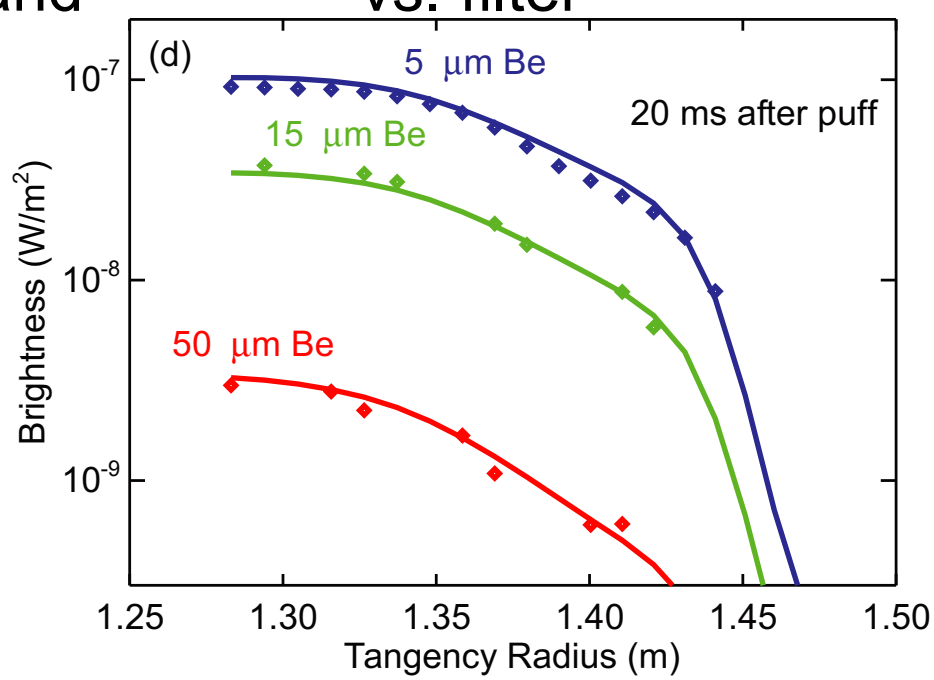

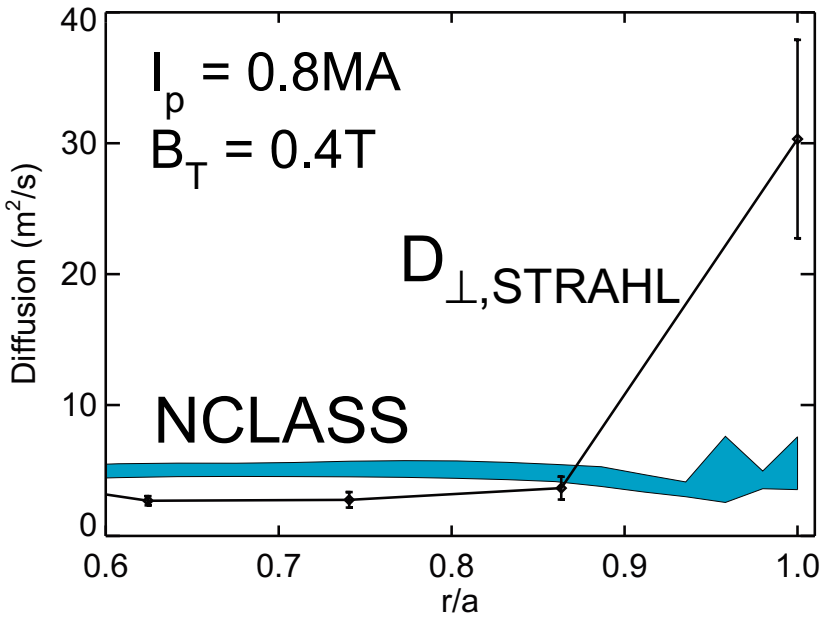

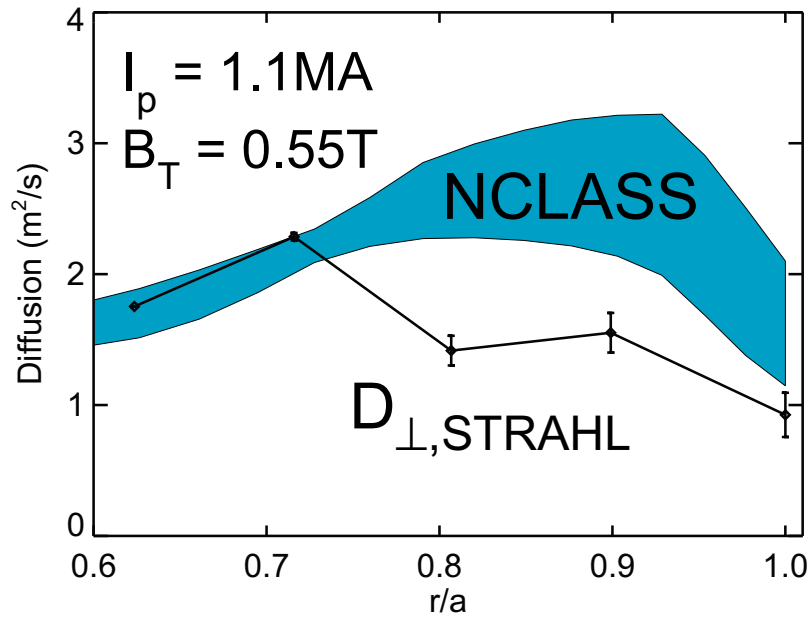

What about the divertor?

- Bulk of previous JHU work focused on main plasma:

  - MHD
  - transport
  - ELMs, boundary physics
  - plasma profiles

- However, divertor has become increasingly important

  - T_e too low for ME-SXR techniques
  - bulk of emission in XUV/VUV wavelengths
  - can we use TGI diagnostic to probe divertor characteristics?

Direct-detection Transmission Grating Imaging Radiometer currently being tested for NSTX-U divertor

D. Kumar, et al., Rev. Sci. Instrum. 83, 10E511 (2012)

CCD detector for improved sensitivity, absolute $P_{rad}(\lambda,x)$

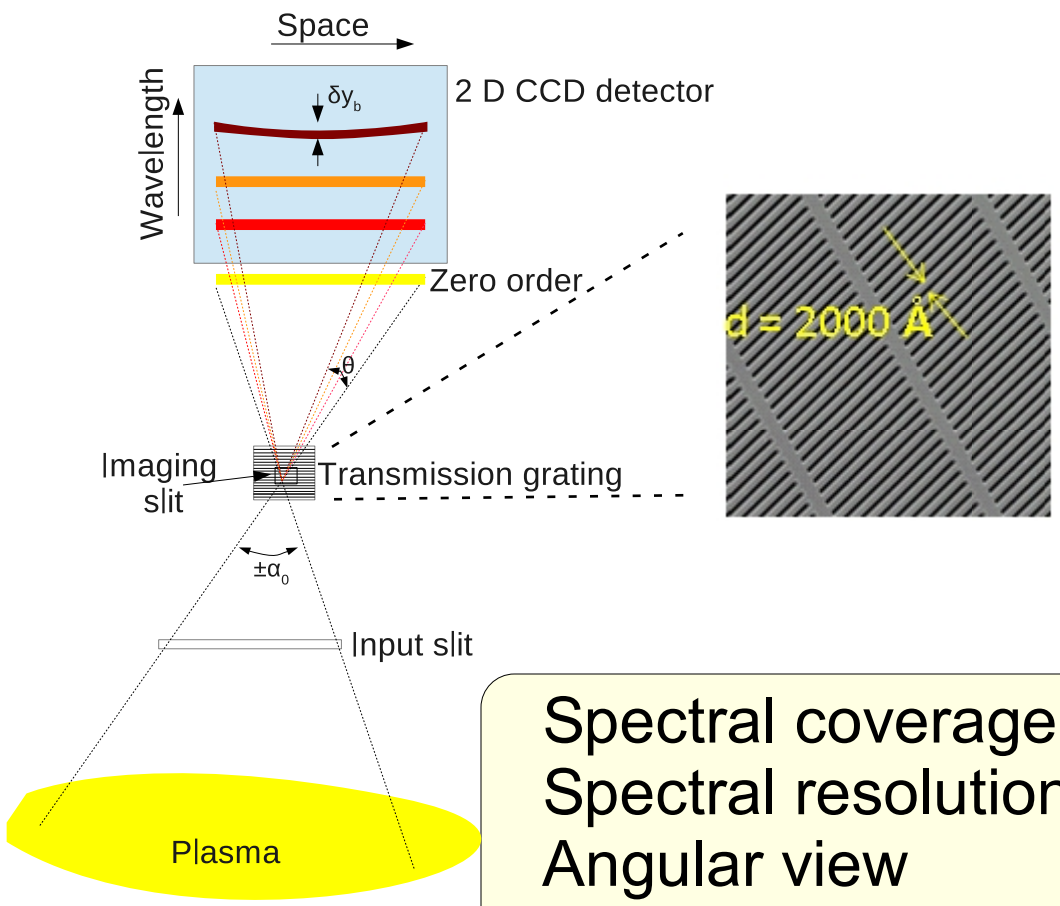

Penning Ion Discharge neon fill gas

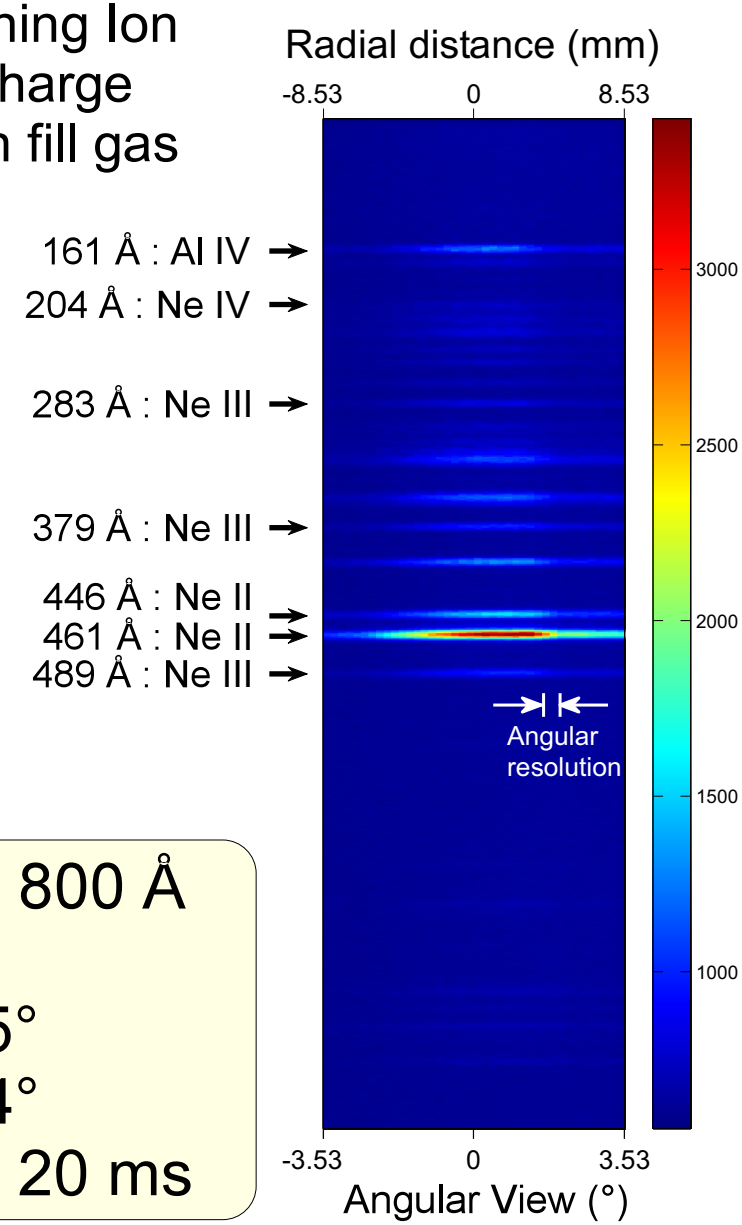

Spectral coverage	60 - 800 Å
Spectral resolution	9 Å
Angular view	±3.5°
Angular resolution	0.44°
Time resolution	10 - 20 ms

Compact TGIR is highly portable, easy to install

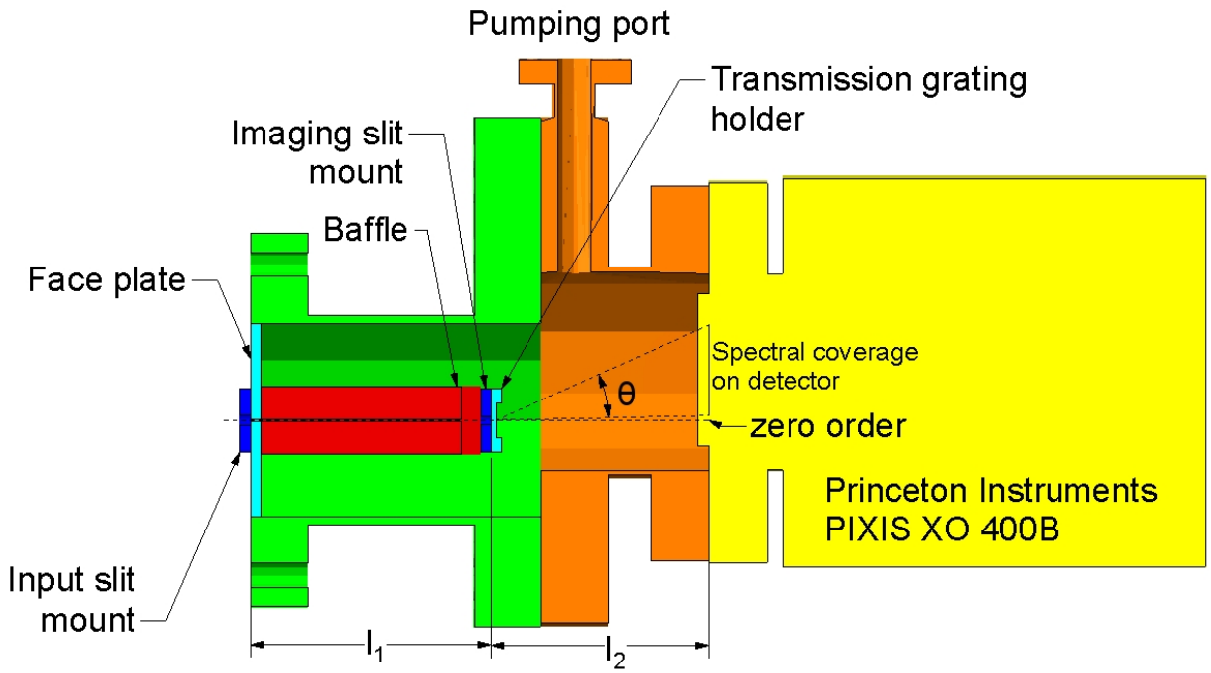

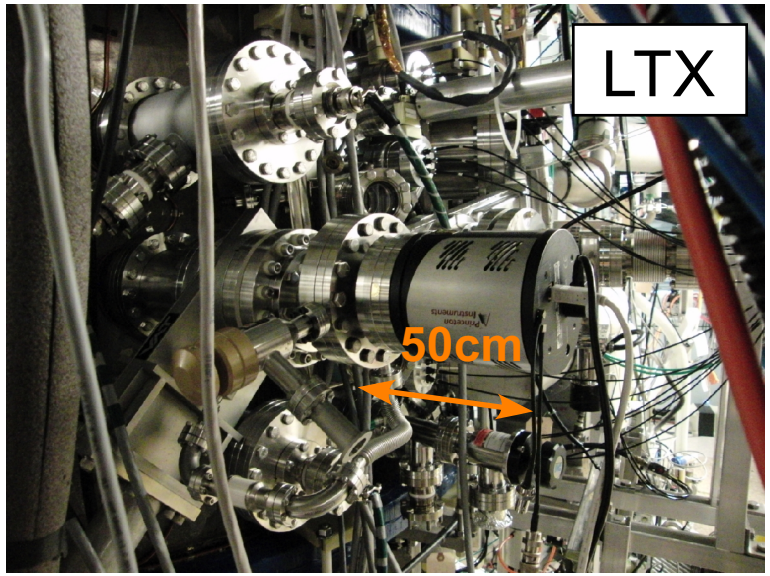

- TGIR currently installed on LTX at PPPL
  - general impurity, P_{rad} survey
  - spectroscopic T_e estimate
  - Fe transport studies (P. Biersdorfer, LLNL, LoWEUS)
  - validate TGIR for use on NSTX-U divertor

Preliminary TGIR results indicate presence of Lithium and Oxygen impurities in LTX discharges

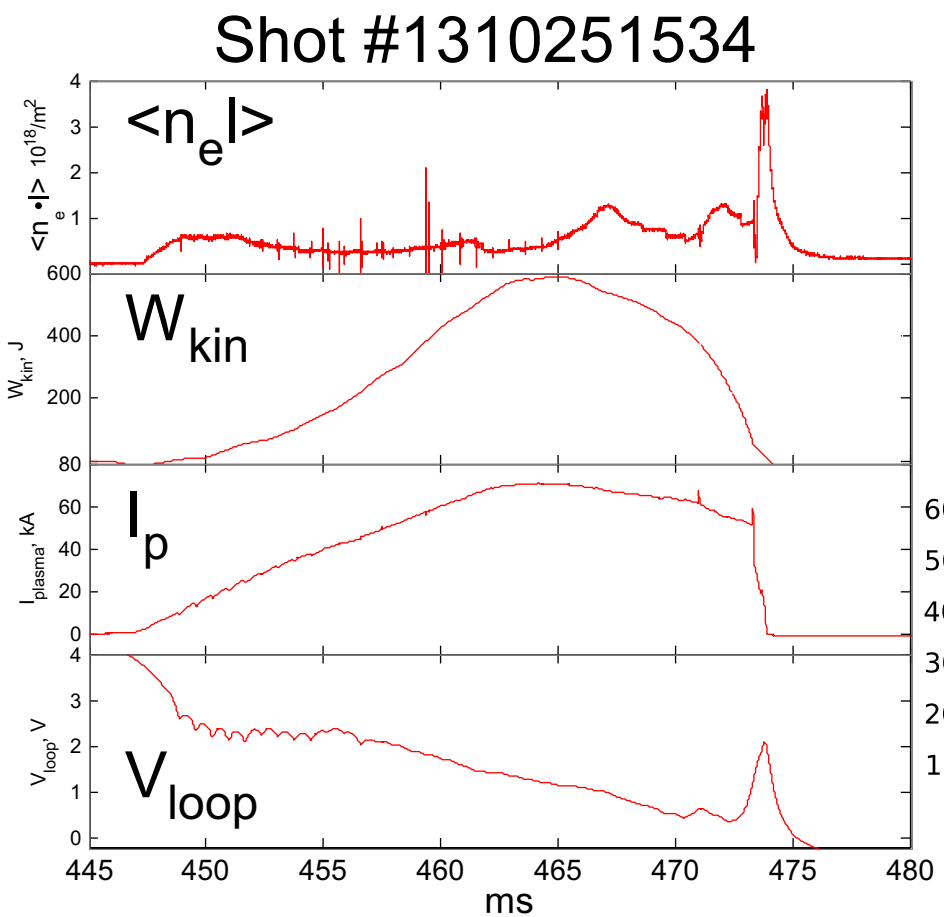

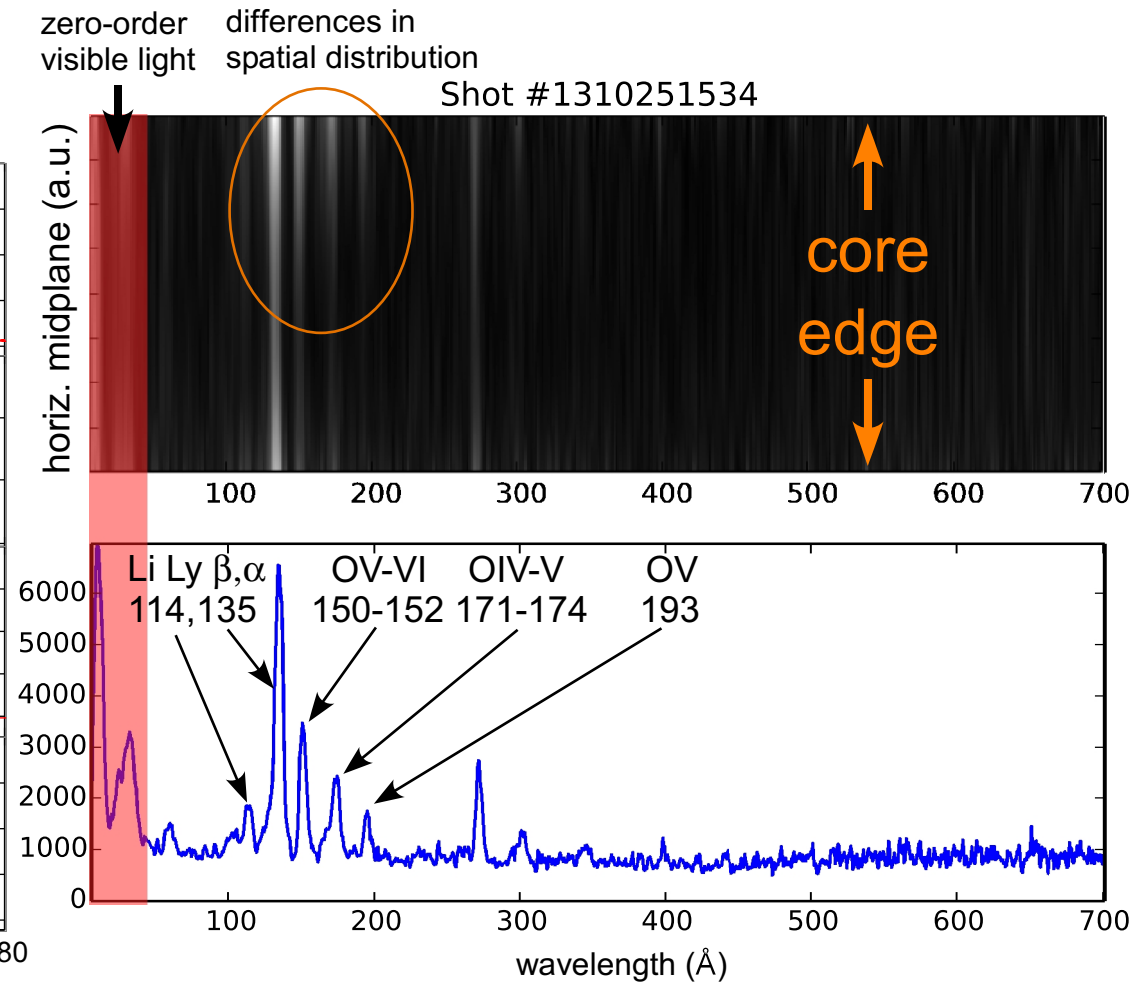

TGIR space-resolved spectrum for LTX discharge

- Noise from high energy X-rays removed using threshold detection
- Initial analysis indicates spatial distribution of emission
  - TGIR integrated over entire discharge

OEDGE NSTX-U divertor modeling with synthetic TGIR diagnostic suggests possibility of T_e, $D_\perp$ measurements

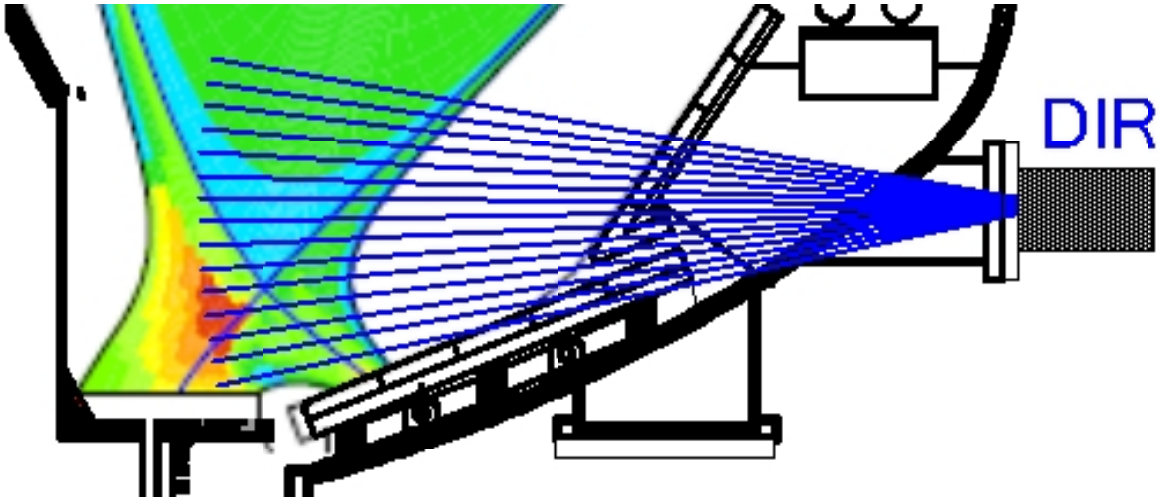

D. J. Clayton, M. A. Jaworski, et al., Rev. Sci. Instrum. 83, 10D521 (2012)

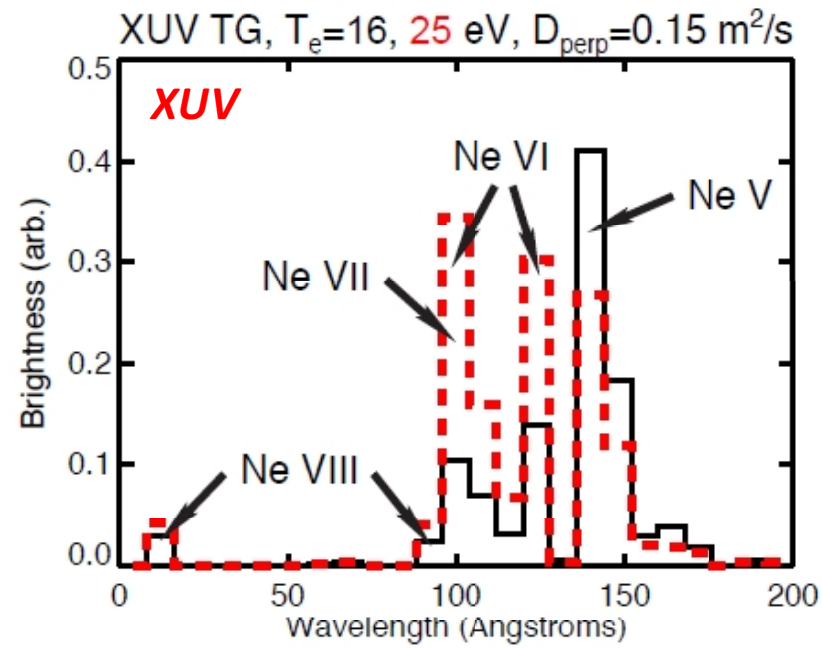

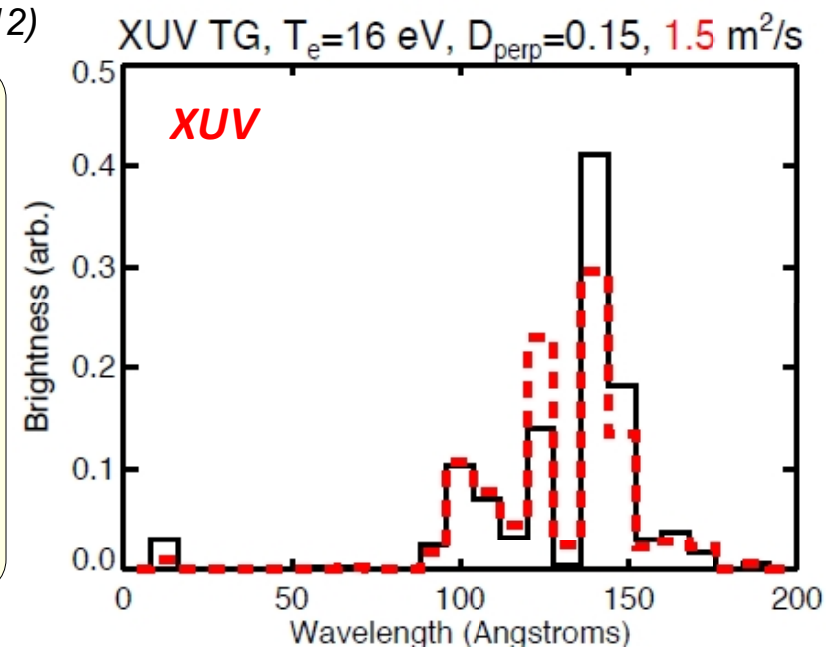

- TGIR will monitor intrinsic C, Li, ...
  - validate sputtering/divertor models
- Can use Ne impurity seeding
  - use charge state emission for T_e
  - good constraint for $D_\perp$ modeling

Spatial resolution of TGIR strongly discriminates between T_e, $D_\perp$ at high divertor plasma temperatures

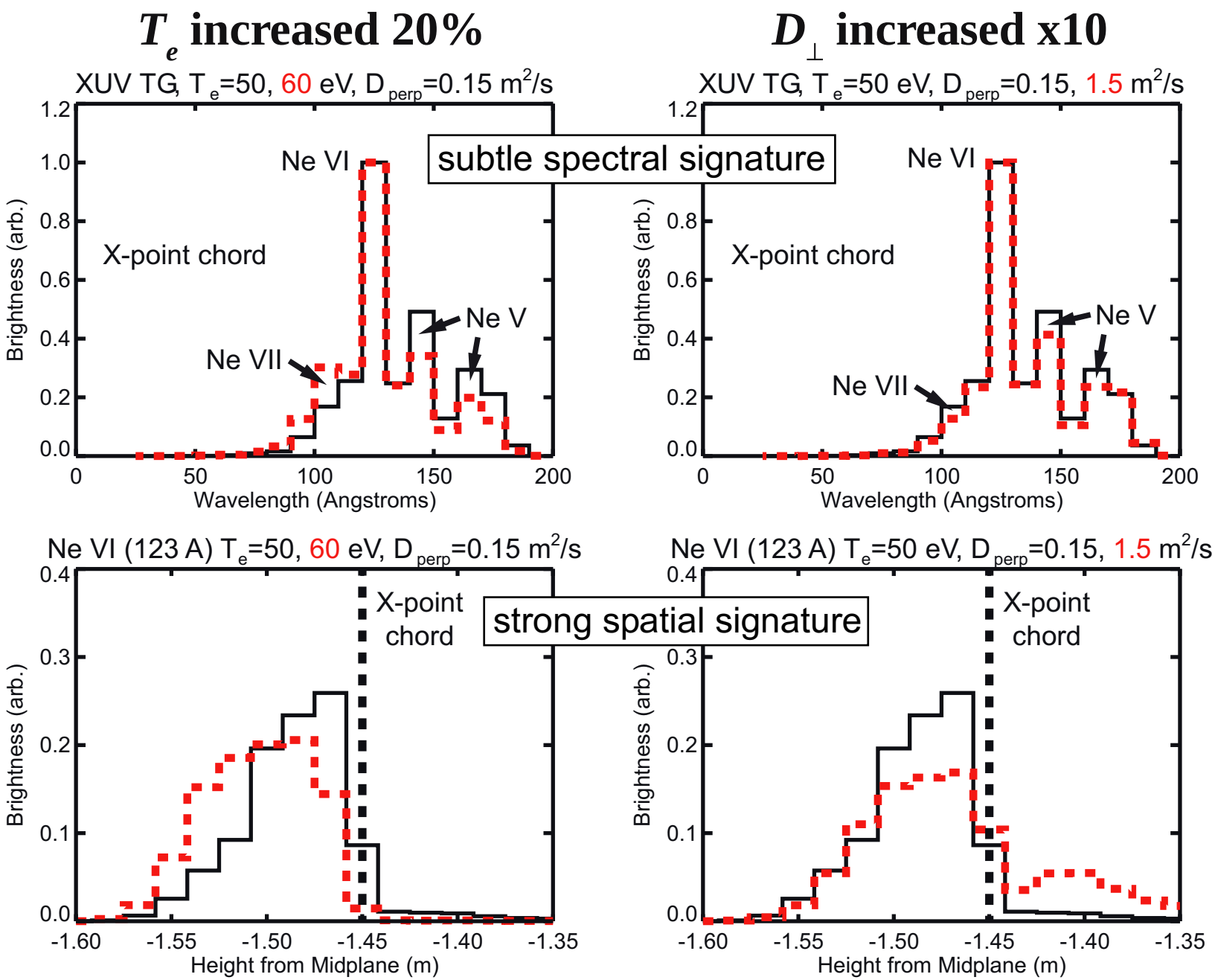

Installation for NSTX-U combines core and high-resolution edge ME-SXR systems

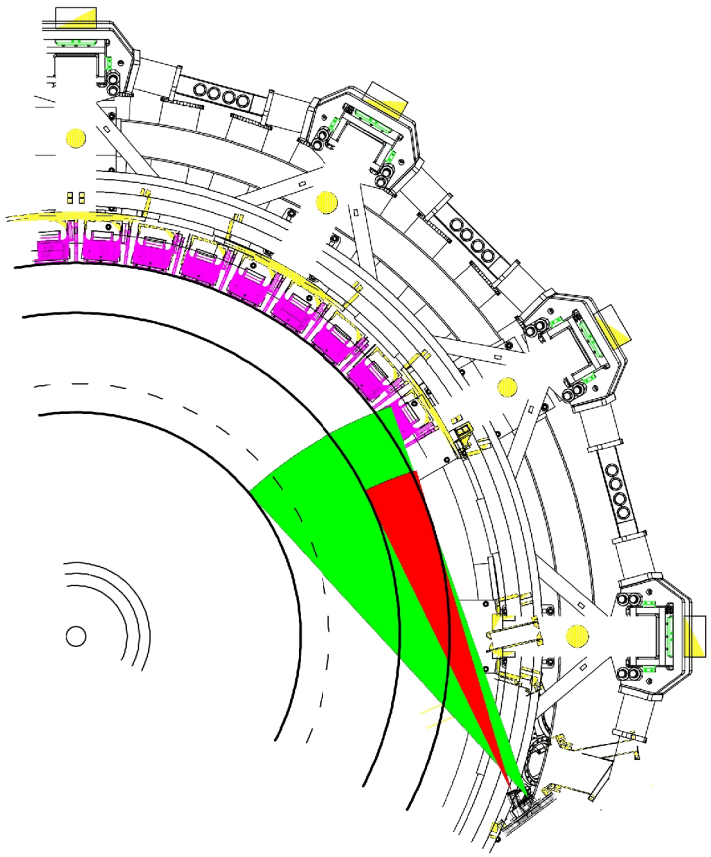

single toroidal location has overlapping core/edge FOV

Core: r_{tan} = 90-150cm, $\Delta r \sim 3$cm
Edge: r_{tan} = 130-150cm, $\Delta r \sim 1$cm

- Arrays use similar filter configuration
  - edge: bolo, Ti 0.3μm, Be 5/15/50μm
  - core: bolo, Be 5/15/50/150μm

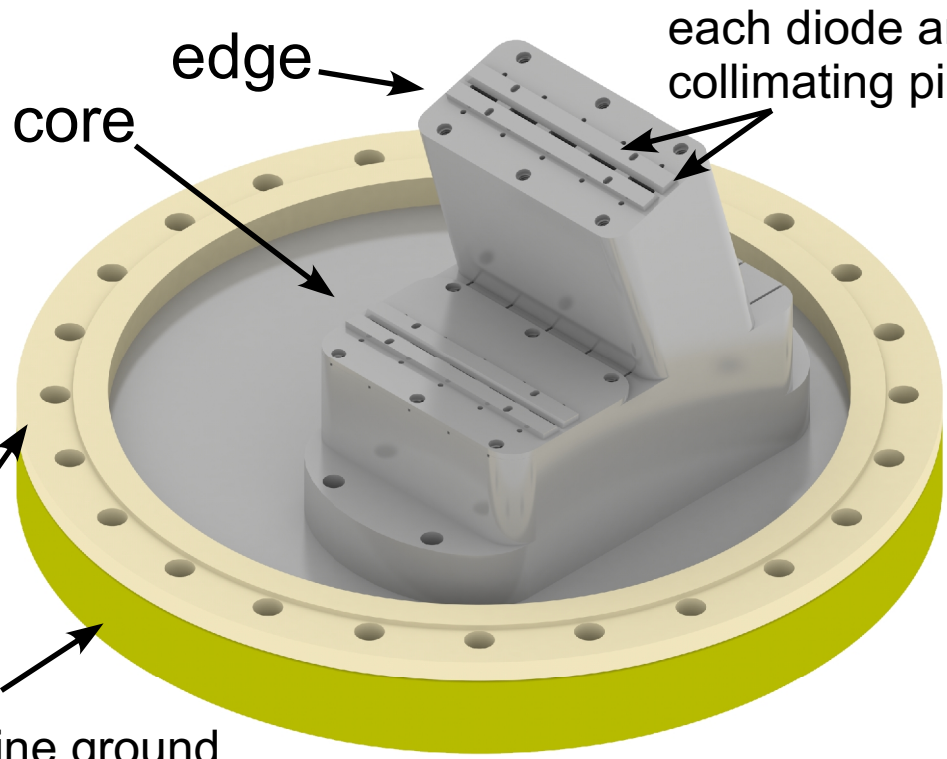

PEEK vacuum gasket and G11 rotatable bolt circle isolate diagnostic and machine ground

Development of modular DAQ couples multi-channel transimpedance amps with microcontroller + ADCs

New acquisition system uses BeagleBone (BB) board as interface for parameters setup, data conversion and streaming.

- 20 channels per board, maximum 5 boards (100 channels) per BeagleBone Board
- 20 kS/s for 100 channels
- individual Lowpass Filters at 10 kHz for each channel
- programmable offset, gain and adjustable bias voltage
- simultaneous sample & hold for 100 channels
- up to 30 (60) seconds of 100 channels acquisition
- real time streaming for data visualization
- external trigger input
- MicroSD card with configuration variables in file config.ini
- debugging messages in console via USB connection
- only one ethernet connection necessary with PC
- LabVIEW program for setup, data acquisition and visualization

ACCENT PRO 2000

http://www.accent.ro

Highly modular DAQ system provides compact deployment, expandability, and low-cost controllers

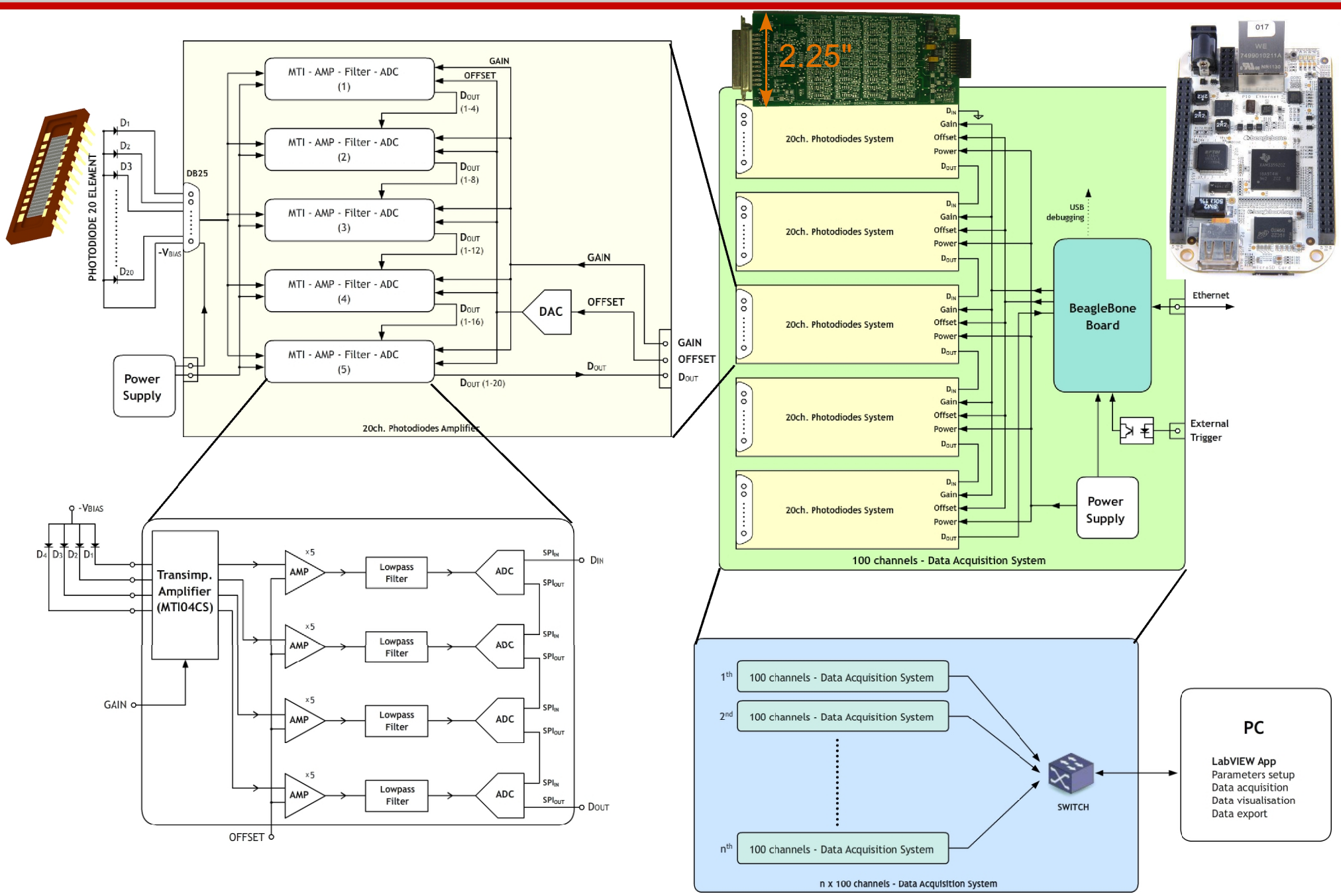

JHU work will continue on NSTX-U, expand techniques to new facilities, and develop new diagnostics for long pulse

- Edge ME-SXR for EAST
  - re-entrant design
  - installation for next run

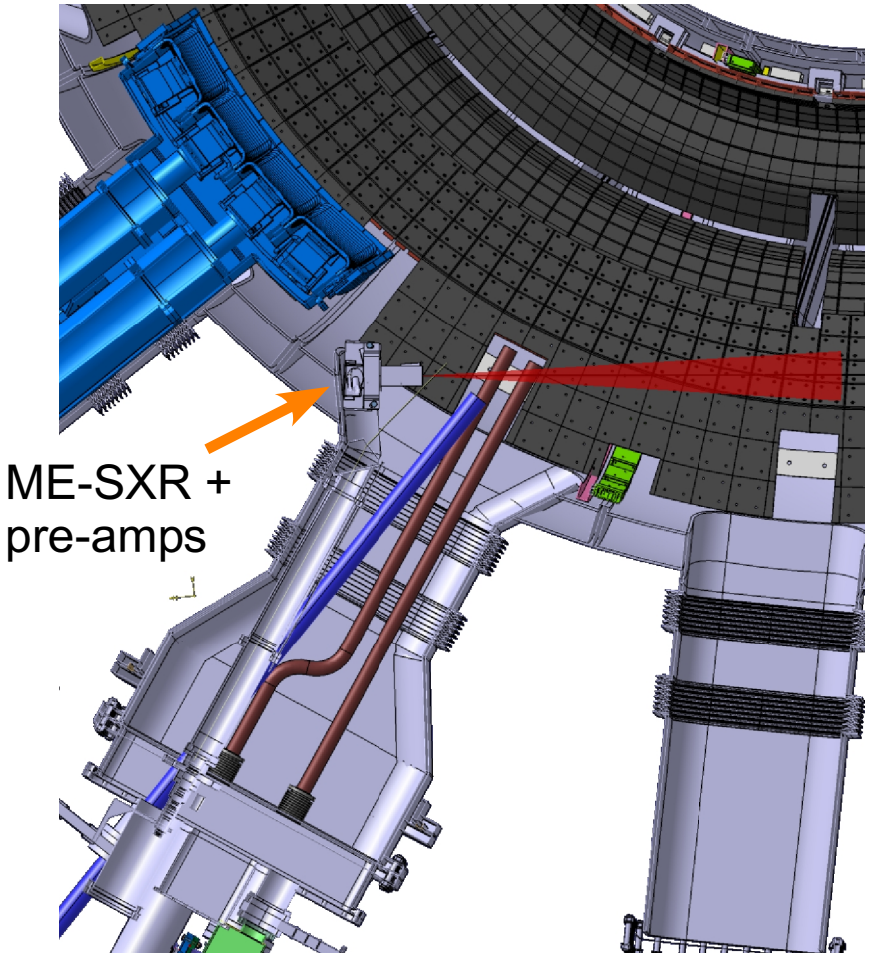

- Bicell sensors detect boundary
  ME-SXR simulation matches EFIT, MPTS measurements

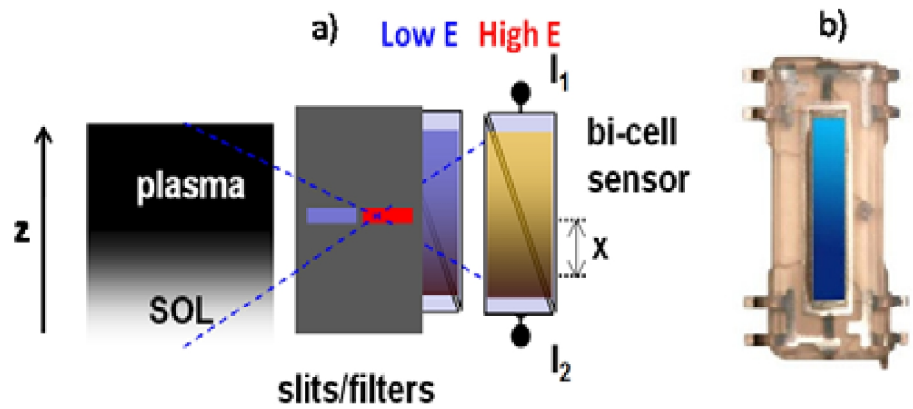

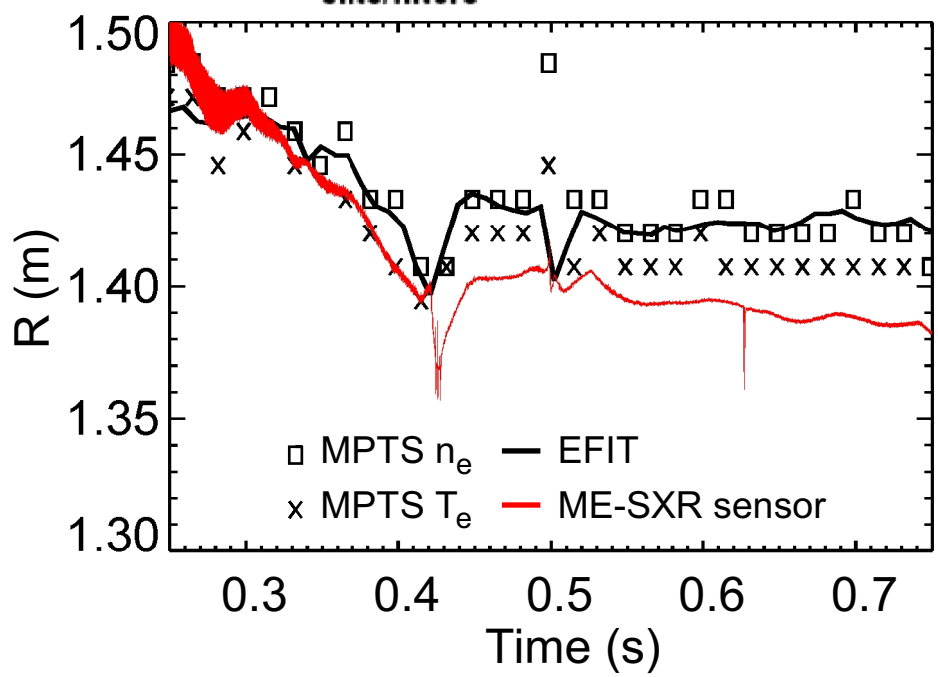

ME-SXR diagnostic techniques and analysis tools can provide important plasma measurements

- The ME-SXR array diagnostic coupled with Neural Network analysis provides a robust measurement of $T_e(R,t)$ on fast time scales
- High resolution SXR measurements provide important measurements of edge boundary, profiles, and phenomena
- $P_{rad}(\lambda,x)$ from a direct detection Transmission Grating Imaging Radiometer is an important tool for divertor measurements and divertor modeling validation

- Development of highly modular ME-SXR/DAQ enables expansion to multiple toroidal locations on NSTX-U, facilitates installation on EAST and other machines